IN-34
35622

NASA Contractor Report 198459

Studies of Two-Phase Flow Dynamics and Heat Transfer at Reduced Gravity Conditions

Larry C. Witte, W. Scott Bousman, and Larry B. Fore
University of Houston
Houston, Texas 77204

February 1996

Prepared for
Lewis Research Center
Under Grant NAG3–510

National Aeronautics and
Space Administration

STUDIES OF TWO-PHASE FLOW DYNAMICS AND HEAT TRANSFER AT REDUCED GRAVITY CONDITIONS

NASA Grant
NAG3-510

UH Account 1-5-54360

Final Report

Larry C. Witte
Professor of Mechanical Engineering
Principal Investigator

W. Scott Bousman
Research Assistant

Larry B. Fore
Post-Doctoral Fellow

Dept. of Chemical Engineering

UNIVERSITY OF HOUSTON
Houston, TX
77204-4792

STUDIES OF TWO-PHASE FLOW DYNAMICS AND HEAT TRANSFER AT REDUCED GRAVITY CONDITIONS

INTRODUCTION 1

EXPERIMENTAL APPARATUS 2
- Flow Loops 2
- Flow Dynamics Test Section 2
- Heat Transfer Test Section 5

FLOW DYNAMICS 7
- Flow Pattern Mapping 9
- Void Fraction Flow Pattern Transition Models 13
- Weber Number-Based Flow Pattern Transition Models 15

SUMMARY OF FLOW DYNAMICS RESEARCH 17

HEAT TRANSFER 17

- Annular Flow 17
  - Calculation of Heat Transfer Coefficients 17
  - Correlation of Heat Transfer 19
  - Pressure Gradient and Film Thickness 20

- Slug Flow 22
  - Data Reduction 22
  - Pressure Gradient Correlation 23
  - Correlation of Heat Transfer 24

SUMMARY OF HEAT TRANSFER RESEARCH 26

REFERENCES 27

NOMENCLATURE 28

APPENDIX I. PUBLICATIONS RESULTING FROM GRANT 30

APPENDIX II. DATA SUMMARY FOR HEAT TRANSFER EXPERIMENTS 31

STUDIES OF TWO-PHASE FLOW DYNAMICS AND HEAT TRANSFER AT REDUCED GRAVITY CONDITIONS

INTRODUCTION

Gas-liquid mixtures occur in a number of situations relevant to on-going and planned space operations. Some examples are the incidental boiling of cryogenic fluids, evaporative heating/cooling systems and power generation systems. In these situations, knowledge of the phase distribution is important for the design of piping systems, separators and other associated units. The prediction of heat transfer characteristics is of particular importance, since the design of such systems for space operations is inherently limited by size constraints.

It was recognized some time ago that predictions of normal-gravity two-phase flows could best be advanced with flow regime-dependent models rather than purely empirical approaches. Following this reasoning, a number of studies have been performed to identify the flow regimes that occur under reduced-gravity conditions and develop criteria for inter-regime transitions (Dukler et al., 1988; Zhao and Rezkallah, 1993; Bousman and Dukler, 1994). The three distinct regimes identified at reduced gravity are bubbly, slug and annular, with transitions of bubbly-slug and slug-annular. Annular flow, where the liquid flows as a thin film along the tube wall and as droplets in a gas/vapor core, occurs over the widest range of gas and liquid flow rates. The largest frictional pressure gradients and heat transfer coefficients occur in annular flow, further increasing the need for good predictive methods.

Annular flows at small enough gravity levels are axisymmetric, much like vertical annular upflows or downflows at earth-normal gravity, in that the liquid film is distributed evenly about the perimeter of the tube. At gas velocities just above the slug-annular transition under reduced gravity, conditions exist which are much unlike those exhibited at normal-gravity. For example, the liquid film can be significantly thicker than possible under the influence of gravity. As the gas velocity is increased and the film becomes thinner, the influence of acceleration on the hydrodynamics decreases relative to shear and pressure forces. Likewise, any differences in heat transfer should decrease with decreasing film thickness.

New experimental results for a 25.4-mm ID tube are reported for air-water, air-water/glycerine mixtures and air-water/Zonyl mixtures. These results augment previous results obtained for a 12.7-mm ID tube, and thus offer an opportunity to determine the

effect of tube diameter, as well as viscosity and surface tension variation on flow patterns in microgravity.

This report also presents new heat transfer, pressure drop and film thickness measurements for air-water and air-50% aqueous glycerine annular flows in a 25.4 mm ID tube at reduced gravity. The hydrodynamics were fully-developed upstream of the 56-cm-long heated section in which local measurements of the heat transfer coefficient were made. The pressure gradient, film thickness and heat transfer coefficients are compared to existing correlations and new relations are developed. Appendix A contains a list of publications that have resulted from this grant to date.

EXPERIMENTAL APPARATUS

Short durations of reduced gravity, less than 1% of earth normal, are created aboard NASA's Zero-G KC-135 and the Learjet 25 aircraft by a series of parabolic trajectories. The aircraft climb and descend between altitutudes of 7.6 and 10.6 km. The data presented here were obtained during microgravity flights using a flow loop designed and constructed at NASA Lewis Research Center and test sections designed and fabricated at the University of Houston.

Flow Loops: Flow loops for the Learjet and KC-135 aircraft are shown schematically in Figures 1 and 2. These flow loops were constructed to provide metered quantities of gas and liquid to the test sections used in these studies (Bousman, 1995). The gas flow rate was controlled with a critically-choked orifice to make the flow rate independent of downstream pressure changes (McQuillen and Neumann, 1995). The uncertainty in the gas superficial velocity measurement was estimated to be 8% over the range investigated in these studies. A steady flow rate of liquid was provided by a pressure-loaded piston in the liquid feed tank. The uncertainty in the liquid superficial velocity measurement was estimated to be less than 10% over the experimental range. The gas and liquid were combined in an annular mixer to produce a gas core surrounded by a liquid film. The two-phase mixture passed through a flow development section prior to entering the test section. At the exit of the test section, the mixture was separated over screens by surface tension and the liquid was recovered for reuse while air was vented into the cabin. Control of flow loop functions as well as data acquisition and storage is accomplished with a dedicated computer in the flow loop rig.

Flow Dynamics Test Section: A 12.7 mm ID test section (shown in Figure 3) for use on the Learjet consisted of a smooth acrylic tube to which several probes were attached. A 25.4 mm ID test section of similar construction (shown in Figure 4) was constructed for use on the KC-135 aircraft. The liquid film thickness and void fraction conductivity probes, shown in Figure 5, were based on the parallel wire conductance

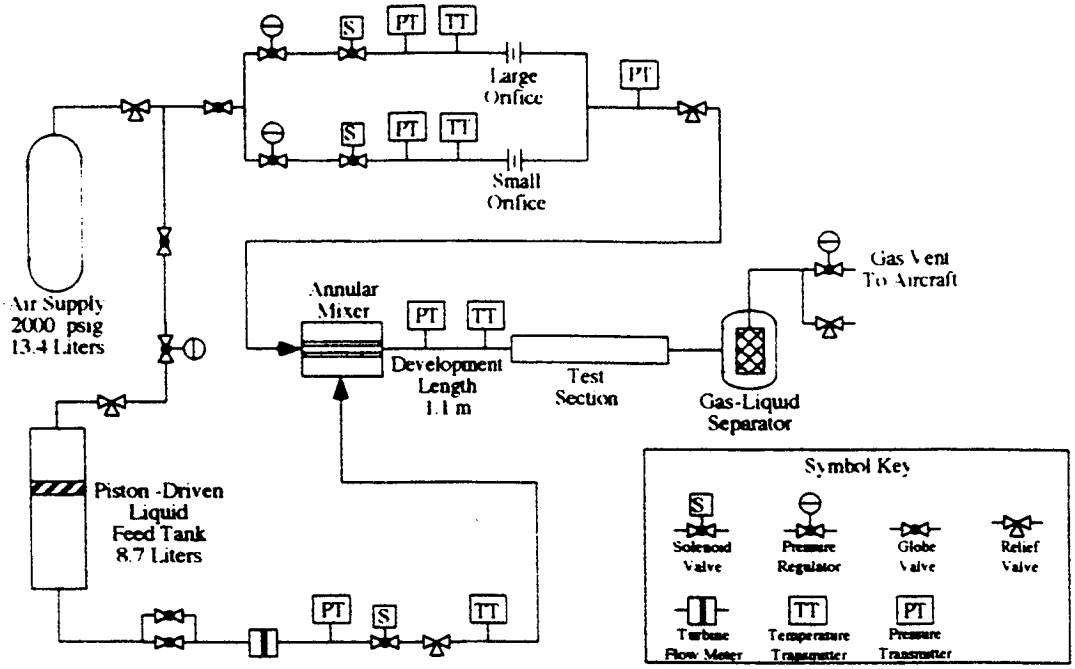

Figure 1. Flow loop used on the NASA Learjet for the 12.7 mm ID test section

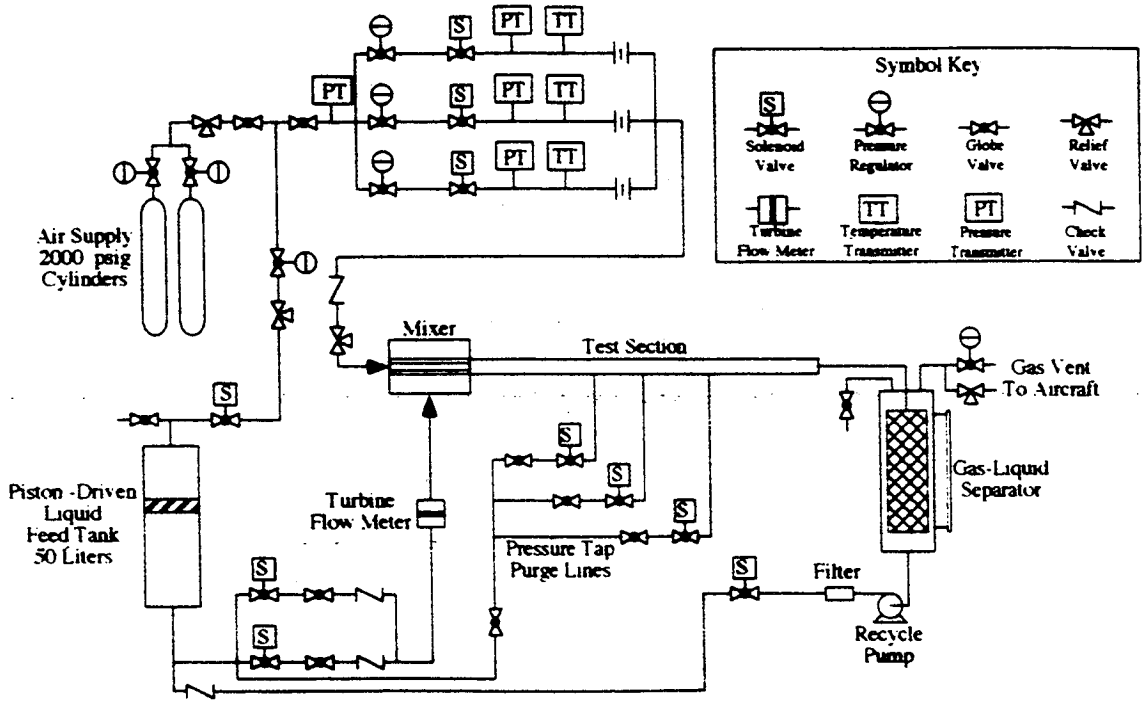

Figure 2. Flow loop used on the NASA KC-135 aircraft for the 25.4 mm ID test section

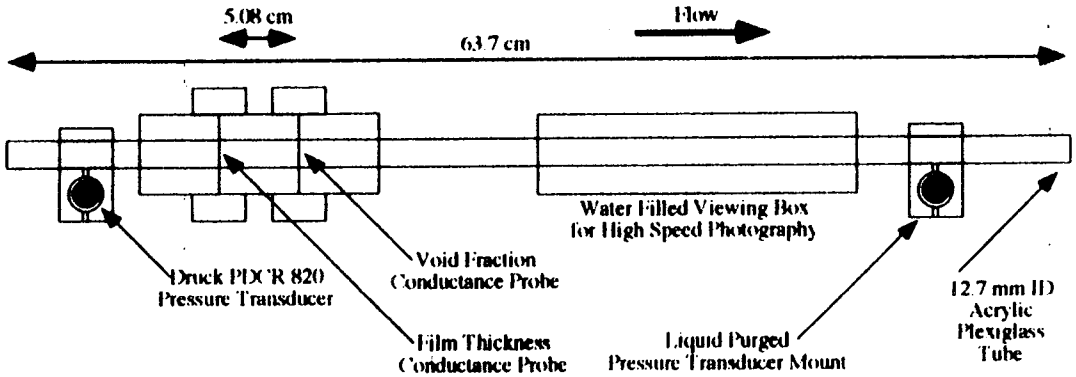

Figure 3. 12.7 mm ID test section

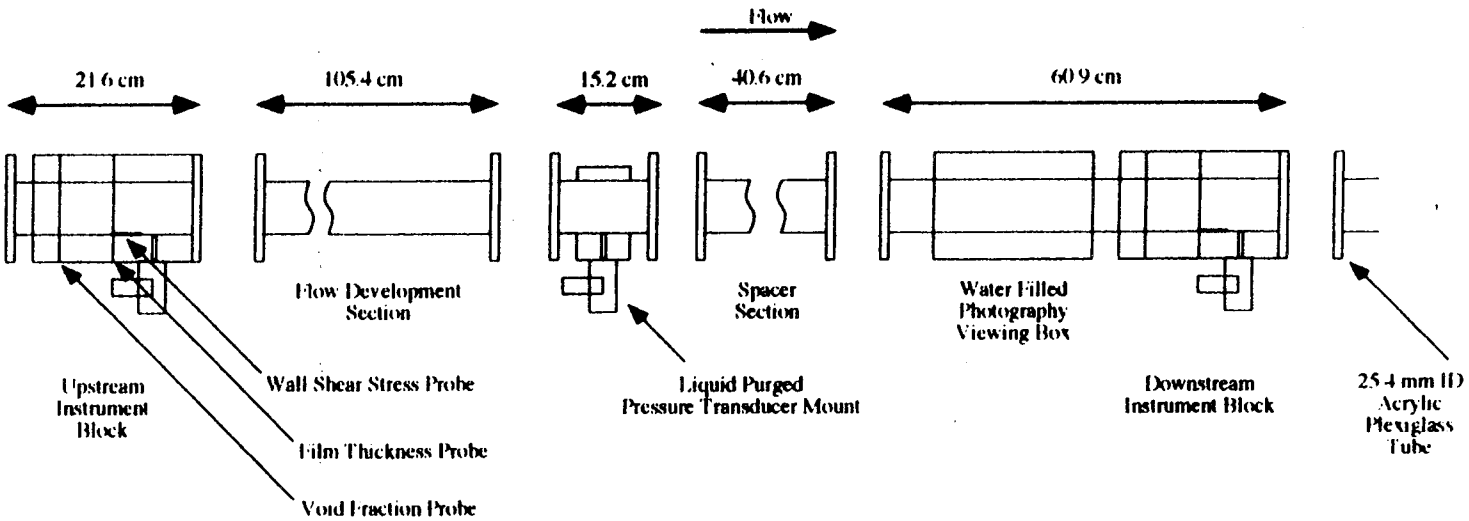

Figure 4. 25.4 mm ID test section

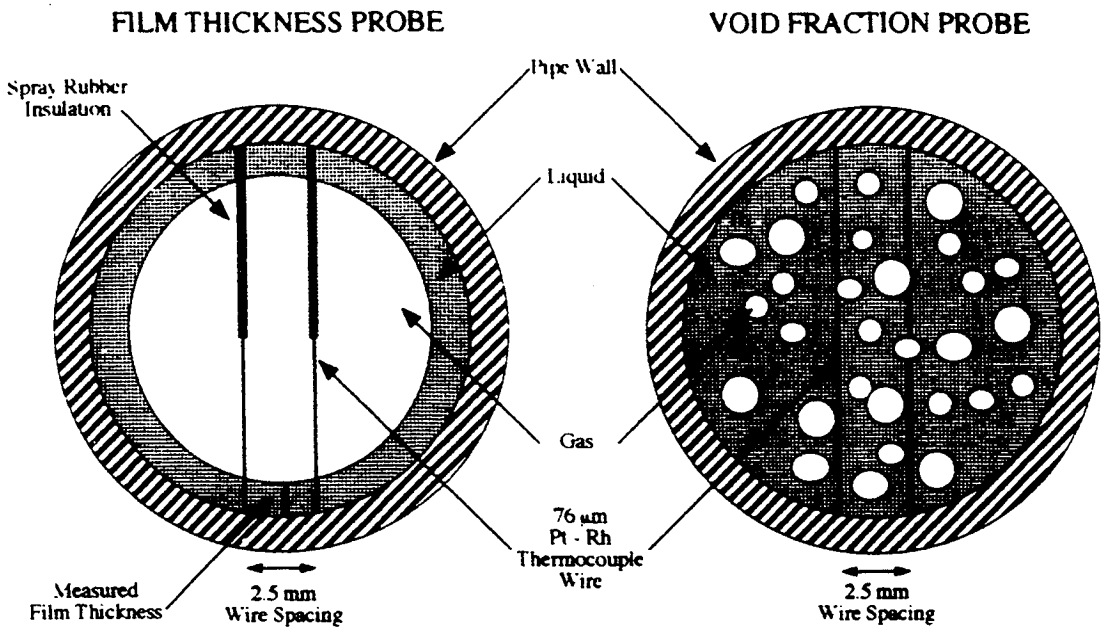

Figure 5. Parallel wire conductance probes for film thickness and void fraction measurements

method described in detail in Bousman, 1995. The probes consist of a pair of closely spaced parallel wires stretched tightly across the tube cross section. High-speed electronics were used to produce a high-frequency alternating voltage (10 kHz) across the wires, allowing measurement of the conductivity between the wires (Lacy, 1992). Conductance probes like this were also used in the heat transfer test section described below. By using aqueous fluids, which were made conductive by adding a small amount of sodium chloride, the conductivity measurement system provides a voltage output which is linearly proportional to the liquid film thickness or void fraction, depending on the calibration. Based on calibration measurement errors and electronic discretization errors, the uncertainty in the void fraction was about $\pm$ 0.01 while the uncertainty in film thickness, d, was about $\pm$ 0.02 mm. The water-filled viewing box allowed for high-speed photography of the flow with minimal refractive distortion. Photographic images of the flow dynamics were acquired at 400 frames/second.

Heat Transfer Test Section: The adiabatic sections between the feed and the heated section and between the heated section and the outlet were constructed of 25.4 mm ID clear acrylic tubing, as shown in Figure 6. The heated tube was constructed of 25.4 mm ID copper tubing. Nylon flanges on the ends of the heated section were machined to make a smooth transition between the two tubing diameters. Two pressure taps for the

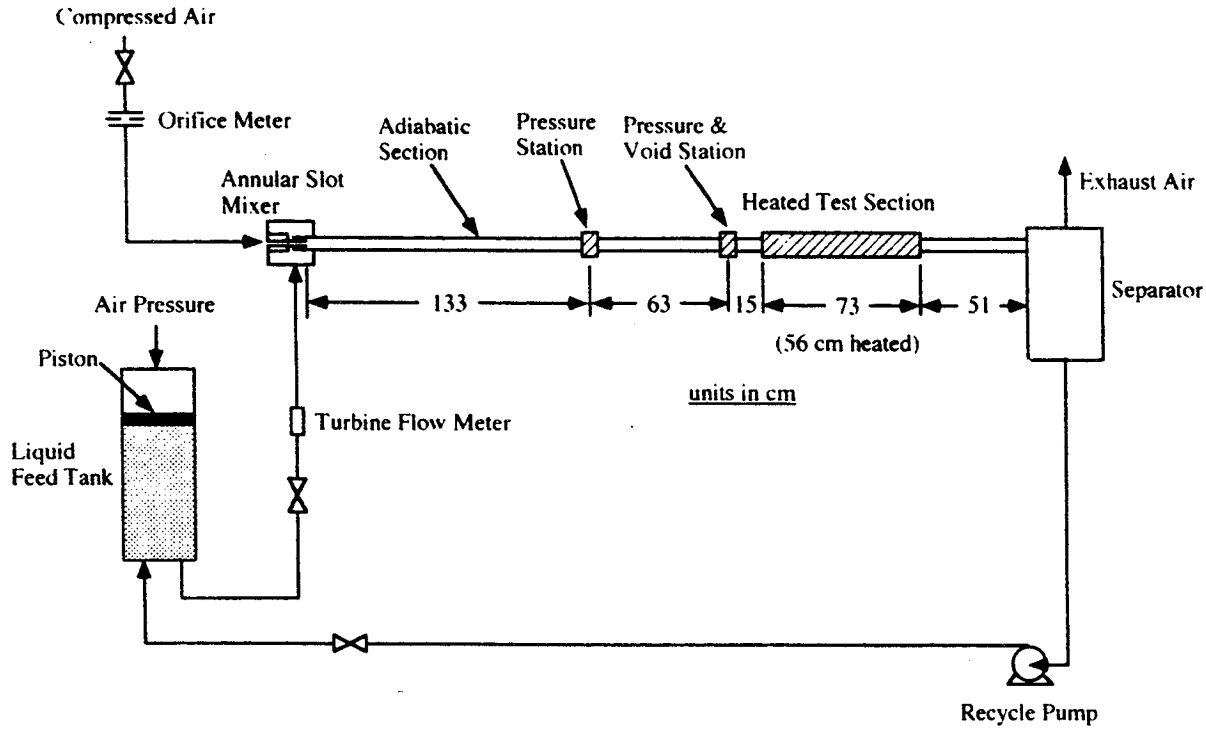

Figure 6. Gas-liquid flow loop for reduced gravity heat transfer experiments

pressure gradient measurement were located upstream of the heated test section at locations 1.33 m and 1.96 m from the feed. This provided flow development lengths of 52.4 and 77.2 tube diameters for each pressure tap, or an average of about 65 diameters. This length should be adequate for an estimate of the fully-developed pressure gradient. A film thickness and a void fraction probe were located at the second pressure tap, separated axially by 50 mm. The heated test section was located 2.11 m from the inlet and has an overall length of 0.73 m, including the adiabatic end-flanges. The length between the feed and heater was chosen to minimize the evaporative heat flux, which is significant near the test section entrance where the air is dry. The exit section leading to the separator was 0.51 m long.

The heated section is a nickel-plated copper tube, with a wall thickness of 1.27 mm wrapped with three 36-ohm (nominal) etched-foil nickel resistance heaters, connected in parallel to 60 Hz AC power The heaters covered all but a 1 cm strip along the length of the copper tube. Wall temperatures were measured with eight 50-ohm nickel RTDs cemented to the tube OD. An Analog Devices 2B31J strain-gage circuit was used to measure the RTD resistances. The entrance bulk temperature was estimated with a nickel RTD mounted inside the nylon flange at the heater entrance. Another RTD was mounted

in a 7-degree expansion section downstream of the heater to provide an estimate of the exit bulk fluid temperature.

The two pressures, film thickness, eight wall temperatures and inlet and outlet temperatures were collected at 1 kHz. Accelerations at two positions along the flow loop were also collected at 1 kHz. Miscellaneous test section temperatures, pressures, and flow rates were collected at 1 Hz.

FLOW DYNAMICS

Identifying the flow patterns in two-phase flows can be difficult, especially for high superficial gas velocities where small flow features can travel in excess of 5 m/s. As a result, flow pattern identification remains partially subjective and this is responsible for some of the discrepancy in flow pattern transitions reported in the literature. In the current study, it was found that a combination of photography and electronic liquid film thickness and void fraction measurements were needed to more objectively identify the flow patterns. Bubbly flow was identified when the gas phase existed as discrete , nearly-spherical bubbles. This flow pattern was usually identified photographically although this flow pattern also possessed a distinctive void fraction time trace. Slug flows were differentiated from bubble flows by the presence of Taylor bubbles which were longer than the tube diameter. This flow pattern was identified using a combination of photography and electronic film thickness traces. A typical microgravity slug flow time trace, shown in Figure 7, clearly shows the presence of Taylor bubbles and liquid slugs. The features of annular flow were difficult to resolve photographically, and these flow

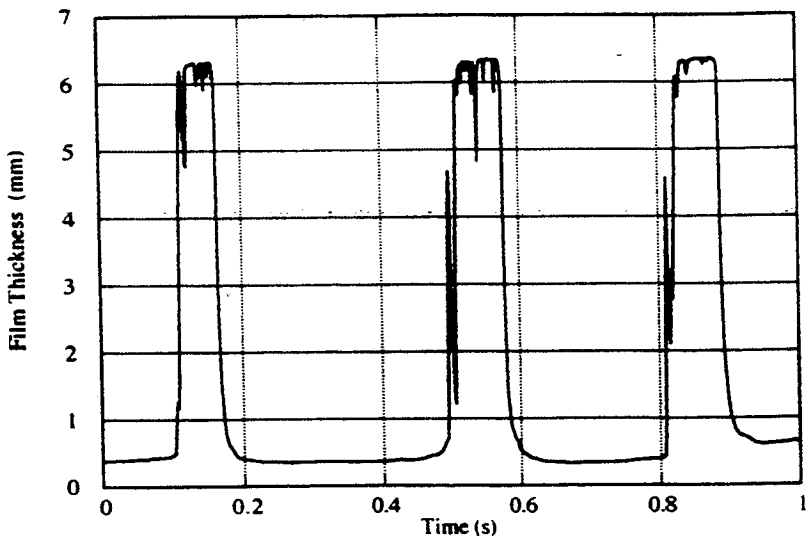

Figure 7. Typical film thickness time series trace for slug flow in microgravity

patterns were usually identified using electronic film thickness time traces, an example of which is shown in Figure 8. This shows the presence of a wavy film with a continuous gas core. Slug flows were differentiated from annular flow by the presence of liquid slugs that bridged the tube. These slugs were often very short and could only be observed using the electronic film thickness measurements. A transitional state between slug and annular flow was also observed, characterized by large amplitude waves which momentarily bridged the tube to form liquid slugs, and then collapsed. An example of a film thickness trace for this transitional state is shown in Figure 9.

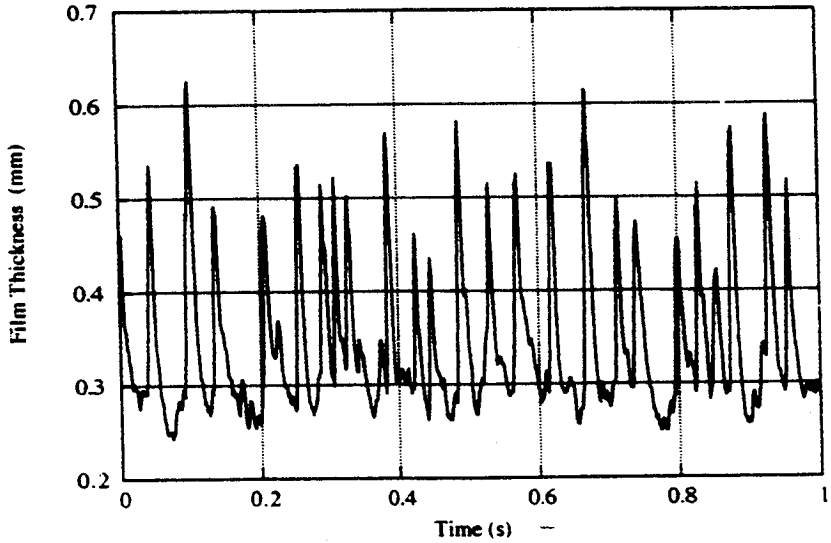

Figure 8. Typical film thickness time series trace for annular flow in microgravity

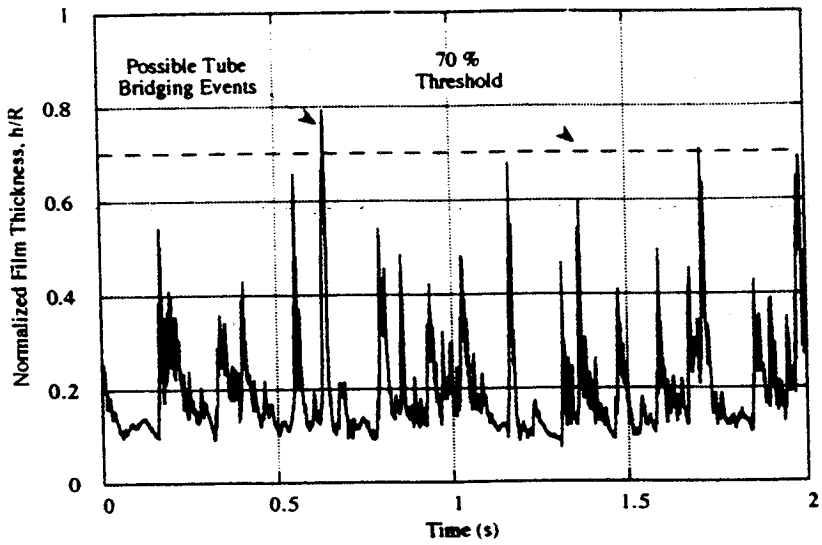

Figure 9. Typical film thickness time series trace for slug-annular transition in microgravity

Flow Pattern Mapping: The experimental apparatus was used to establish flow pattern maps in microgravity as a function of liquid viscosity, surface tension and tube diameter, which are the key parameters affect the flow pattern maps. Three liquids were tested (all at 21 ± 2 C): water (μ = 1 cP, σ = 72 dynes/cm), 50-50 wt% water/glycerine (μ = 6 cP, σ = 63 dynes/cm), and water/Zonyl FSP (μ = 1 cP, σ = 21 dynes/cm). Zonyl FSP (Dupont) is a powerful surfactant which in low concentrations can lower the surface tension without affecting other physical properties of the liquid. Flow pattern maps were determined for these liquids and air in 12.7 and 25.4 mm ID tubes.

The flow pattern maps are shown in Figures 10 through 15. A comparison of Figures 10 and 13, shows that the change in tube diameter leads to a shift in the bubble-slug transition to lower valus of U_{GS}, and thus void fraction, for the air-water system. For the air-water/gylcerine and air-water/Zonyl FSP systems, the change in tube diameter produced no significant change in the location of the bubble-slug transition. For all three fluid systems, tube diameter had little effect on the location of the slug-annular transition.

Comparison of the air-water and air-water/glycerine flow pattern maps shows that a six fold increase in the liquid viscosity produced no significant change in the location of either flow pattern transition, indicating that liquid viscosity is not a major factor affecting pattern transitions. Comparison of the air-water and air-water/Zonyl FSP maps shows that reducing the surface tension results in a shift in the bubble-slug transition to higher void fraction suggesting that surface tension plays a role in the bubble-slug transition mechanism. The change in surface tension had no significant effect on the slug-annular transition.

The air-water flow pattern map for the 12.7 mm ID tube is in good agreement with the results of Dukler et al., 1988, and Janicot, 1988. This result is expected since all three studies were done with similar apparatus and techniques.

The location of the transition between bubble and slug flow on the air-water flow map of Colin, 1990 for a 30 mm ID tube compares well with the 25.4 mm ID air-water flow pattern map of this study.

The results of Huckerby and Rezkallah, 1992, for air-water in a 9.525 mm ID tube show fair agreement with the 12.7 mm tube air-water results of this study. The Huckerby and Rezkallah map shows the bubble-slug transition nearly independent of the gas superficial velocity, U_{GS}, which is contrary to the findings of the present study. The slug and annular regions of both flow maps are similar. The Zhao and Rezkallah, 1993, study for air-water in a 9.525 mm ID tube shows the bubble-slug transition region to be significantly different than that of Huckerby and Rezkallah, 1992, or the present 12.7 mm

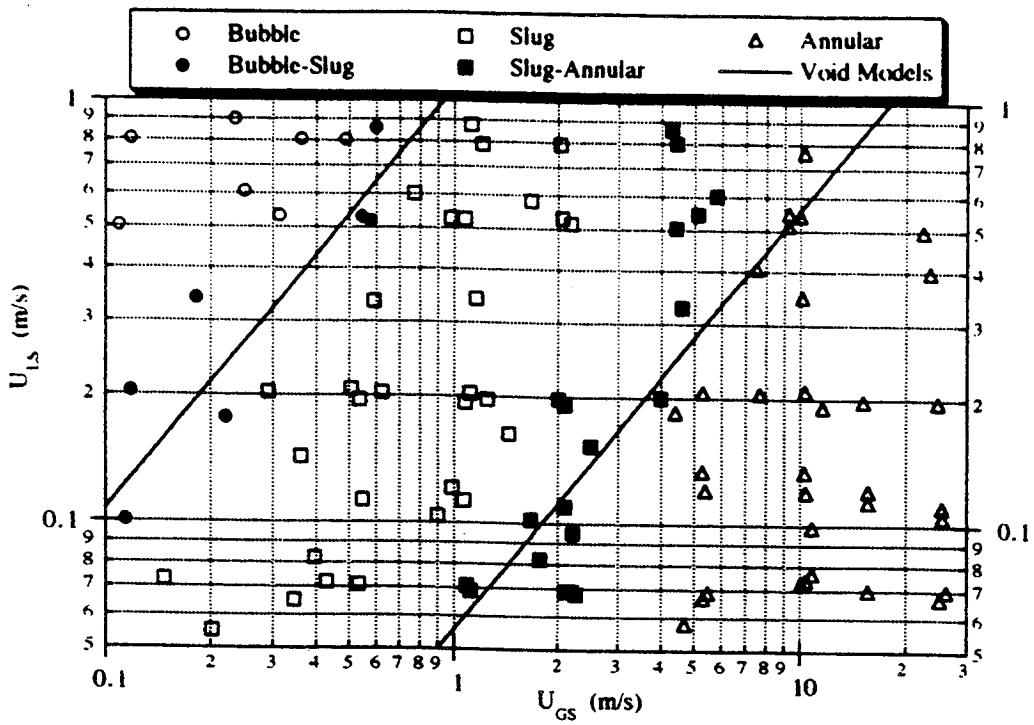

Figure 10. Microgravity flow pattern map for air-water in a 12.7 mm ID tube

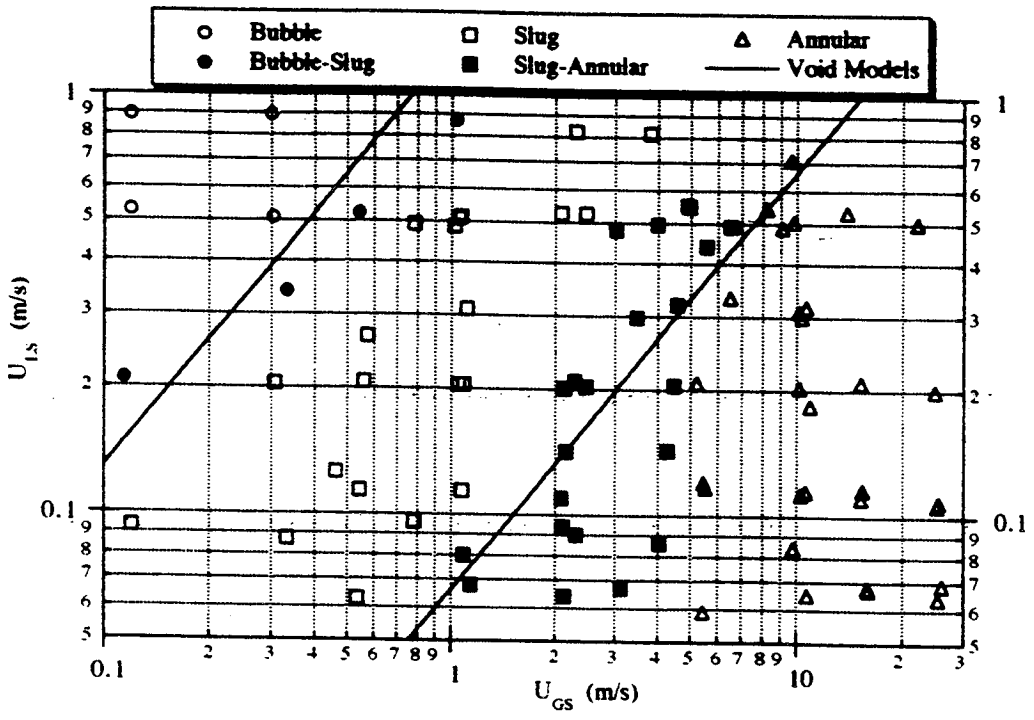

Figure 11. Microgravity flow pattern map for air-water/glycerine in a 12.7 mm ID tube

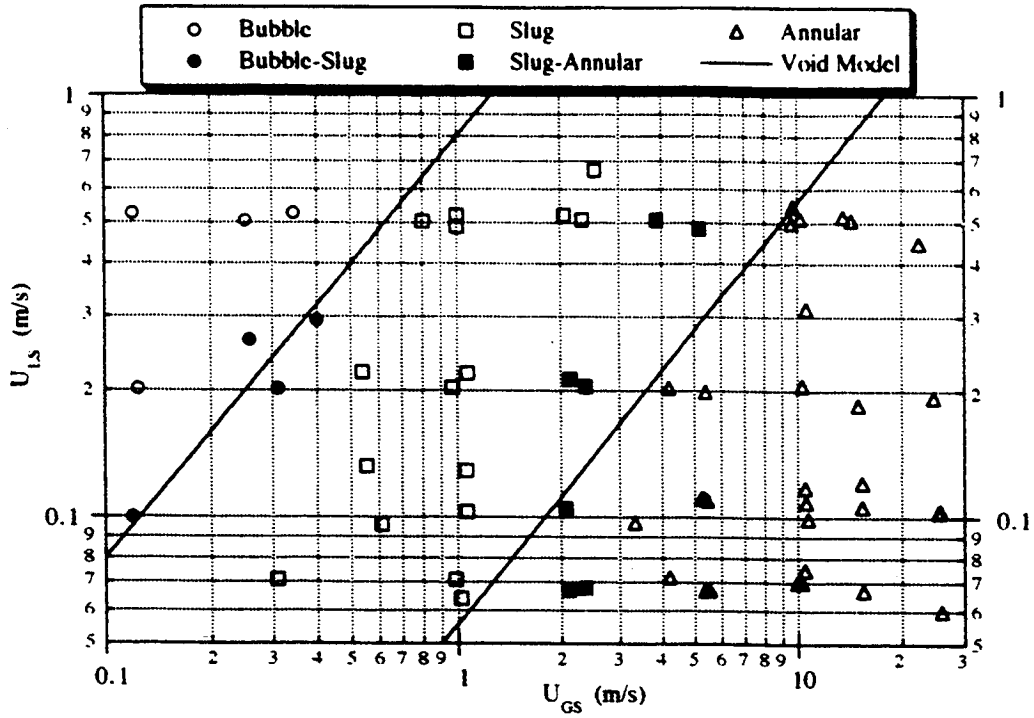

Figure 12. Microgravity flow pattern map for air-water/Zonyl FSP in a 12.7 mm ID tube

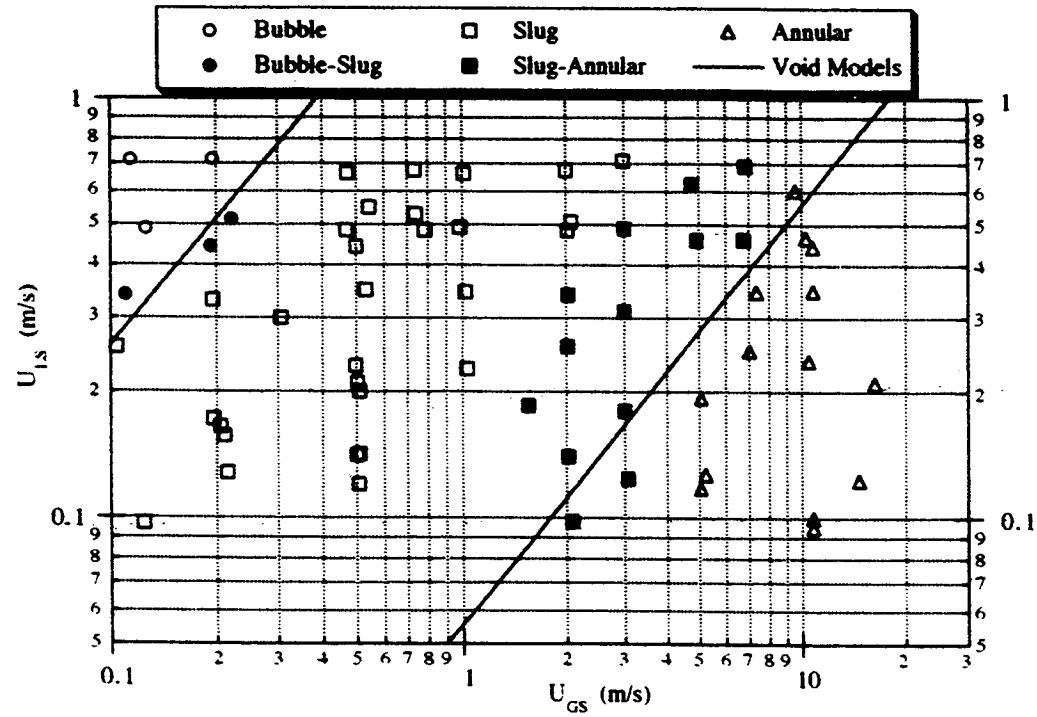

Figure 13. Microgravity flow pattern map for air-water in a 25.4 mm ID tube

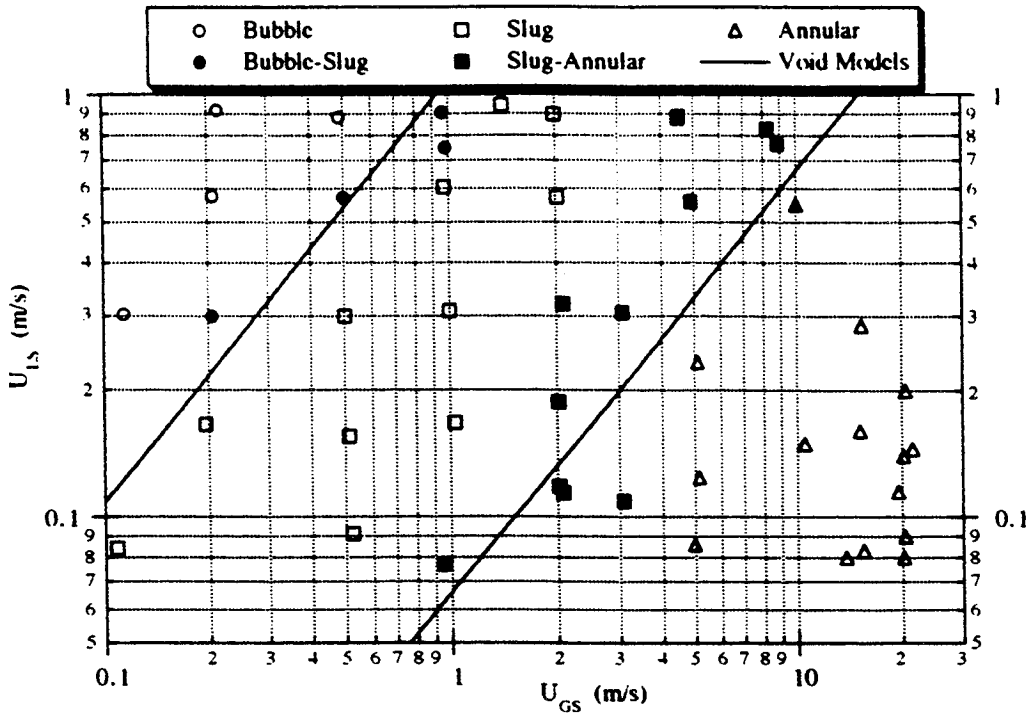

Figure 14. Microgravity flow pattern map for air-water/glycerine in a 25.4 mm ID tube

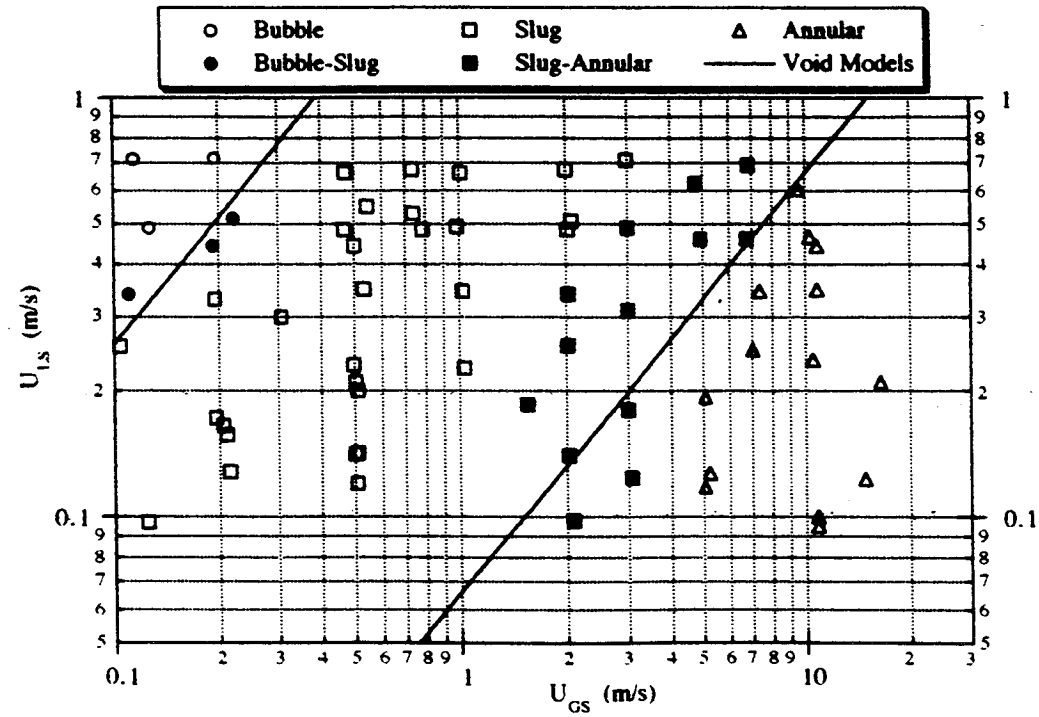

Figure 15. Microgravity flow pattern map for air-water/Zonyl FSP in a 25.4 mm ID tube

ID air-water map. The cause of this discrepancy is unexplained. The location of the Zhao and Rezkallah slug-annular transition is in good agreement with the present results.

Void Fraction Flow Pattern Transition Models: In addition to establishing flow patterns maps, it is useful to develop models that predict the location of the transitions on the maps. For microgravity gas-liquid flow pattern transitions, two approaches have been suggested: a void fraction criteria from Dukler et al., 1988, and a Weber number criteria from Zhao and Rezkallah, 1993. Both were examined in relation to the current study.

The void fraction based model for the bubble-slug transition was developed by examining the high-speed movie images of the experiments near the transition. These films suggested that the transition from bubble to slug flow occurred when spherical bubbles became so densely packed that they touched and coalesced. This implies that the transition occurs at a constant void fraction. The maximum packing density of rigid spheres is 52%, which imposes an upper limit on the transition void fraction. However, oscillations in the shape and position of the bubbles due to turbulence give the bubbles a larger diameter and allow for coalescence at lower void fractions.

The mean void fraction values measured for bubble-slug transition flows in a 12.7-mm ID tube were found to lie in a distinct range between those of the bubble and slug flow experiments. The center point of this range was used as the characteristic void fraction for the transition. Since adequate void fraction measurements were not available for the experiments conducted in the 25.4-mm ID tube, the void fraction of each transition run was estimated using the Drift-Flux model (Zuber and Findlay, 1965) with a distribution parameter determined from the 12.7-mm ID tube experiments (Bousman, 1995). From these estimated void fractions, the transition void fraction was determined for each flow pattern map. The transition void fraction value for each tube diameter and fluid system is shown in Table 1.

The Drift-Flux model with a drift velocity of zero (due to the lack of buoyancy between phases in microgravity) leads to

$$U_{LS} = \frac{(1 - C_o\langle\alpha\rangle)}{C_o\langle\alpha\rangle} U_{GS} \tag{1}$$

The distribution coefficient C_0 was determined to be 1.21 for microgravity gas-liquid flows using experimental void fraction measurements (Bousman, 1995). Using this in conjunction with the transition void fraction values of Table 1 yields lines of constant void fraction on the flow pattern maps which represent the predicted bubble-slug transition.

Table 1

Transition Void Fraction Values for the Bubble-Slug Transition

Fluids	Tube Diameter (mm)	Transition Void Fraction
Air-Water	12.7	0.40
Air-Water/Glycerin	12.7	0.36
Air-Water/Zonyl	12.7	0.46
Air-Water	25.4	0.23
Air-Water/Glycerin	25.4	0.40
Air-Water/Zonyl	25.4	0.40

The bubble-slug transition predicted from the void fraction matching criteria is superimposed on the flow pattern maps in Figures 10-15. As shown, these lines of constant void fraction separate the bubble and slug regions of the flow map, which is expected since these models were derived from the data. With the exception of the air-water flow pattern map for the 25.4-mm ID tube, the bubble-slug transition occurs at a void fraction of about 40%.

The decrease in the transition void fraction for the air-water system in the larger diameter tube is also present in the flow patterns presented by Colin, 1990, for air-water in a 40-mm ID tube. To better understand this result, the movie films of the experiments near the transition were examined for both the small and large tubes. In the 25.4-mm tube, the gas-liquid bubble interfaces were in a continuous state of fluctuation while those in the 12.7-mm tube under the same flow conditions were more stable. These oscillations in the larger tube, which can be attributed to turbulence, give the bubbles a larger effective diameter thus increasing the probability of contacting nearby bubbles. The result is a transition to slug flow at a lower void fraction. This effect was not observed in the air-water/glycerin experiments in the larger tube due to a reduction in turbulence. The reduced surface tension in the air-water/Zonyl experiments should reduce the probability of coalescence when bubbles contact each other and this may explain why the decrease in transition void fraction was not observed for this system in the larger tube when the strong bubble oscillations were present.

A void fraction slug-annular transition model was developed by Bousman, 1995, using force balances to determine a void fraction relationship for annular flow. By

equating this with the slug flow void fraction expression developed from the Drift-Flux model, a void fraction matching condition is imposed as the transition criterion. This model predicts that the transition occurs at the line of constant void fraction when both the gas and the liquid phases are turbulent. A transition value of $\alpha = 0.8$ was determined for all flow maps using the 12.7-mm tube. The transition model for turbulent gas and laminar liquid is more complex, but the predicted void fraction occurs at a nearly constant value of U_{GS}. This model over-predicted the transition void fraction in the turbulent liquid region, possibly due to the problems in accurately determining the pressure gradient in the unstable slug-annular transition region.

The results of Bousman, 1995, showed that the void fraction matching slug-annular transition model was very sensitive to the transition void fraction value used. If a line of constant void fraction at α=0.75 is used instead of that predicted from the more rigorous model, good separation of the slug and annular regimes is obtained for the air-water and air-water/Zonyl FSP flow pattern maps for both tube diameters. A reasonable criterion for the air-water/glycerine maps is α=0.70. These constant void fraction criteria are superimposed on the experimental flow pattern maps in Figures 10-15.

Weber Number-Based Flow Pattern Transition Models: Zhao and Rezkallah, 1993, proposed using a nondimensional approach to modelling flow pattern transitions. Their proposal involved using the Weber number defined as

$$We = \frac{\rho U^2 D}{\sigma} \tag{2}$$

This represents the balance between inertial and surface tension forces. Flow pattern maps in terms of gas and liquid Weber numbers were presented by Zhao and Rezkallah and showed that the slug to slug-annular and slug-annular to annular transitions occurred at approximately We_{GS}=1 and We_{GS}=20 respectively.

Flow pattern data collected in the present study were replotted in terms of gas and liquid Weber numbers as shown in Figures 16 and 17, for air/water which is typical of other fluids tested. As shown, the boundaries of the slug-annular region appear to occur at approximately constant values of We_{GS} for We_{LS}<100 but not at higher values of We_{GS}. This suggests that there might be merit to the concept of Weber number-based transition modelling although another mechanism, responsible for the deviation at the higher values of We_{LS}, might also affect flow pattern transitions.

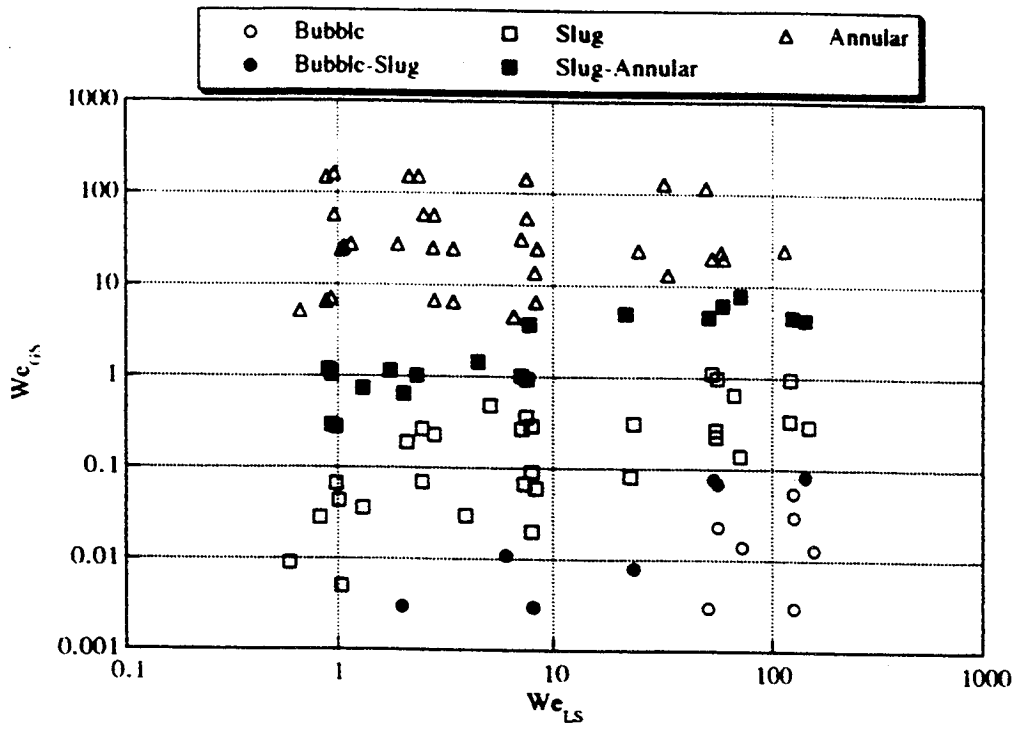

Figure 16. Microgravity Weber Number flow pattern map for air-water in a 12.7 mm ID tube

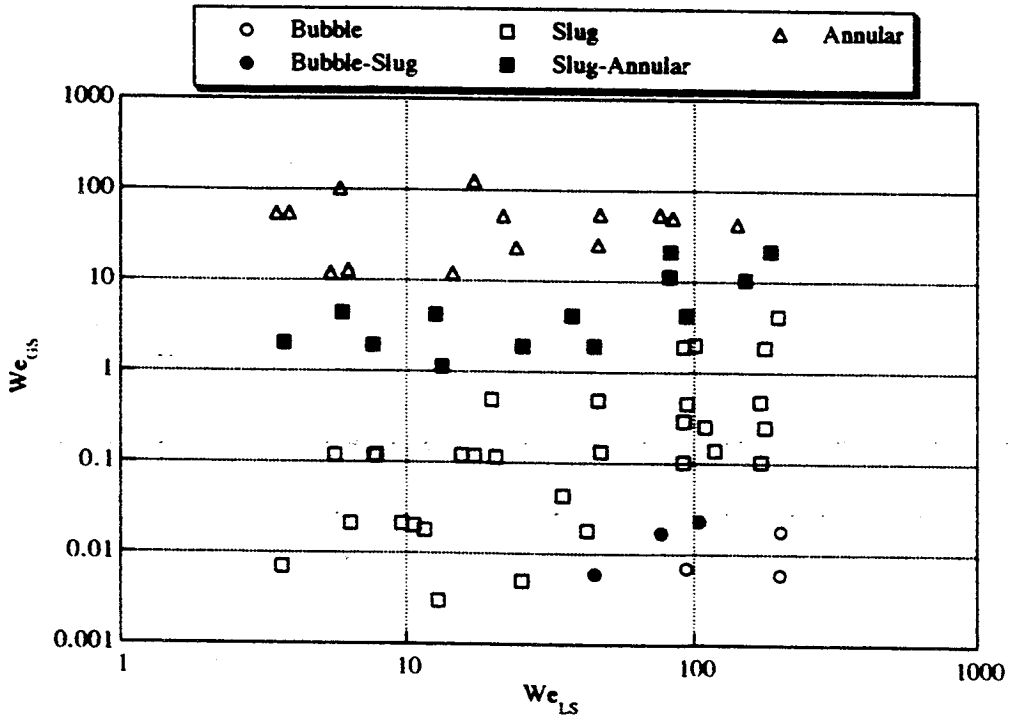

Figure 17. Microgravity Weber number flow pattern map for air-water in a 25.4 mm ID tube

SUMMARY OF FLOW DYNAMICS RESEARCH

The ability to predict gas-liquid flow patterns is crucial to the design and operation of two-phase flow systems in the microgravity environment. Flow pattern maps have been developed in this study which show the occurrence of flow patterns as a function of gas and liquid superficial velocities as well as tube diameter, liquid viscosity and surface tension. The results have demonstrated that the location of the bubble-slug transition is affected by the tube diameter for air-water systems and by surface tension, suggesting that turbulence-induced bubble fluctuations and coalescence mechanisms play a role in this transition. The location of the slug-annular transition on the flow pattern maps is largely unaffected by tube diameter, liquid viscosity or surface tension in the ranges tested. Void fraction-based transition criteria were developed which separate the flow patterns on the flow pattern maps with reasonable accuracy. Weber number transition criteria also show promise but further work is needed to improve these models.

HEAT TRANSFER

Because of fundamental differences in slug and annular flow, different techniques of data reduction were required. Thus it is appropriate to discuss slug and annular flow separately in what follows. All the data were collected for a 25.4 mm ID tube using air and two fluids, water and 50-50 wt % water/glycerine. Pressure drop, heat transfer, film thickness and void fraction data were collected for each flight experiment. A complete listing of the heat transfer data is given in Appendix B.

Annular Flow

Calculation of Heat Transfer Coefficients: The steady-state wall temperatures were estimated for each run by averaging the latter portions of the time series, where the wall temperatures appeared to be at asymptotic values. Depending on flow conditions, the wall temperatures varied widely among experiments. The film thickness was estimated by

$$\delta = \left[\frac{Re\,\mu^2}{2\rho\tau} \right]^{1/2}, \tag{3}$$

obtained from the flat-film laminar velocity profile and definition of the Reynolds number. Even though the film was turbulent for most of the test conditions, equation (3)

was used to provide a uniform treatment for all conditions and for comparison with the theoretical transient analysis. The stress, τ, was estimated with an axial momentum balance averaged over the tube cross-section as

$$\tau = -\frac{D}{4}\nabla P, \tag{4}$$

and the wall heat flux was defined by the heater power divided by the inner area of the heated tube. The local Nusselt number ($Nu=h\delta/k$) is then simply

$$Nu = \frac{1}{\theta_W - \theta_B}, \tag{5}$$

where q_W and q_B are the dimensionless wall and bulk temperatures, respectively. In this formulation, the time-averaged wall heat flux is assumed to be uniform. The bulk temperature was estimated from an enthalpy balance on the liquid as

$$T_B = T_{IN} + \frac{q_w}{\Gamma C_p} \tag{6}$$

Several local Nusselt numbers calculated with equation (5) are shown in Fig. 18. The thermal entry length is shorter than that predicted from laminar, flat-film theory, probably

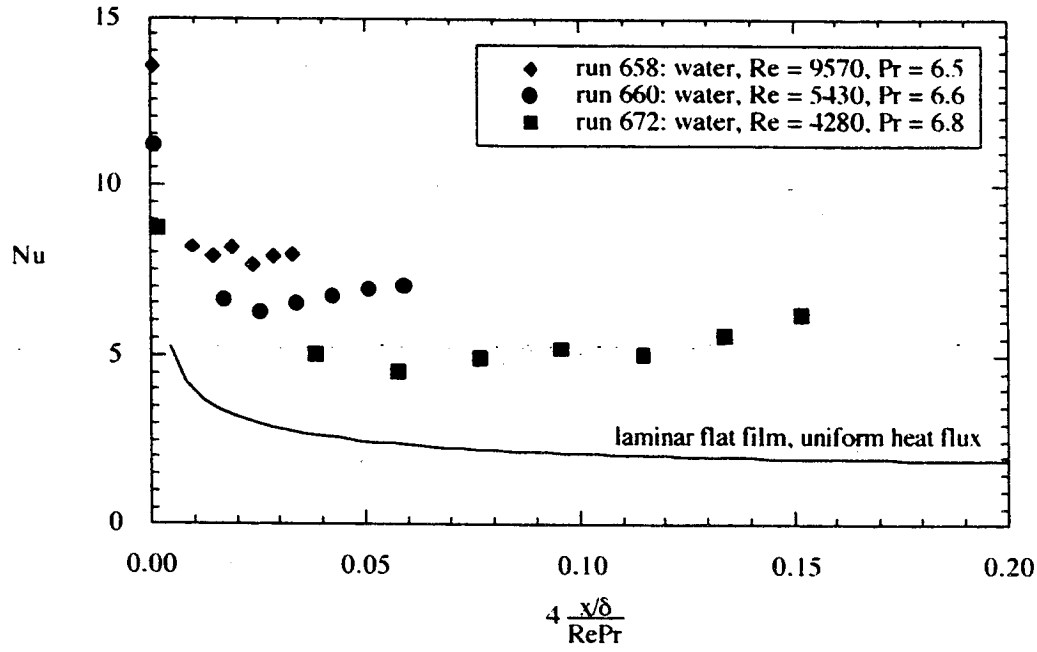

Figure 18. Estimated Nusselt numbers along heated tube for annular flow

due to the higher-than-predicted heat transfer coefficients, wave motion and film turbulence. For the water run 658, it is fairly easy to interpret the asymptotic Nusselt number since the wall temperatures reached steady state values in the experimental period. It is more difficult for runs 660 and 672. The downstream temperatures did not reach steady values, thus the computed Nusselt numbers at the tube exit are larger than the asymptotic value. However, an estimate of the asymptotic Nusselt number is available by examining the portion of the tube that did reach thermal equilibrium, which typically included all but the two temperatures farthest downstream. This strategy is used for all runs in which downstream lengths of the tube did not reach thermal equilibrium.

Correlation of Heat Transfer: Several empirical methods for correlating the two-phase heat transfer coefficient have been proposed. These differ significantly from the more analytical approach of correlating film thickness-based Nusselt numbers with Reynolds number, but the generality of empirical methods allows extension to other flow patterns besides annular.

It was found that the current data do not agree well with the Rezkallah and Sims (1987) turbulent correlation, which is based on the void fraction, or with Shah's (1981) correlation, which includes a gravity term.

Correlation of annular flow data with the analytical flat-film model makes more sense, provided a good estimate or measurement of δ is available. To diminish any bias in the δ measurement that translates to Nu, the laminar and Kosky (turbulent) (1971) correlations shown in Figure 21 in the succeeding section are used to estimate δ for use in the Nu calculation. These δ correlations agree very well with normal-gravity vertical downflow data (Andreussi and Zanelli, 1979) and with a significant portion of the present data. Figure 19 presents Nusselt numbers computed with these predictions of δ, using the liquid Re and measured pressure difference. Both fluids follow the same dependence in this case, correlating according to

$$Nu = A\, Re^{n}\, Pr^{1/3} \left[\frac{Pr}{Pr_w} \right]^{1/4}, \qquad (7)$$

with A=0.0152 and n=0.684. The ±20% lines quantify the scatter fairly well, which is somewhat larger for water than for 50% glycerine. The use of δ correlations in this case results in a single dependence of Nu on Re and Pr, but more experimental data are clearly needed to reduce the uncertainty in equation (7) prior to its use in critical applications.

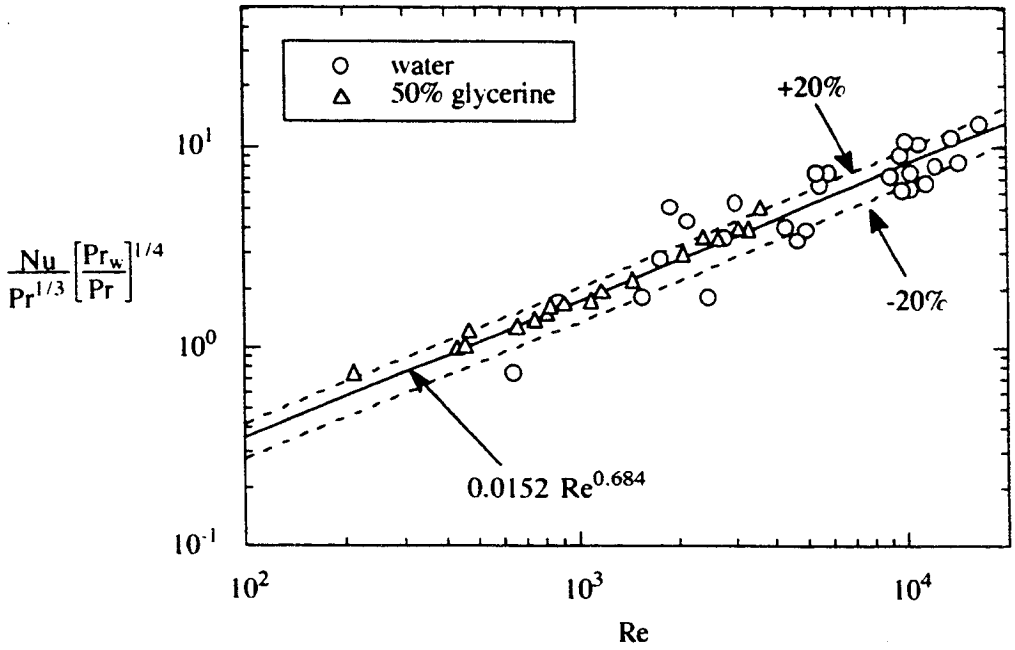

Figure 19. Correlation of Nusselt numbers using film thickness correlations for annular flow

Pressure Gradient and Film Thickness: The experimental pressure gradient is correlated first with the Lockhart-Martinelli correlation (Lockhart and Martinelli, 1949). The parameters X^2 and ϕ_G are defined as

$$X^2 = \frac{\nabla P_L}{\nabla P_G} \tag{8}$$

and

$$\phi_G^2 = \frac{\nabla P_{TP}}{\nabla P_G}. \tag{9}$$

The single-phase pressure gradients are calculated with the friction factors, f=16/Re for Re ‹ 2000, and f = 0.08/Re$^{1.4}$ for Re › 2000. The resulting correlation is shown in Figure 20. For nearly all the conditions, the agreement is adequate with the Chisholm and Laird (1958) equation,

$$\phi_G^2 = 1 + 20X + X^2, \tag{10}$$

which has been previously established by Bousman (1994). The ±25% lines are added to quantify the scatter in the data. At least 10% of this scatter is attributed to experimental error, since Bousman found agreement within 15% for a smaller diameter (12.7 mm) tube.

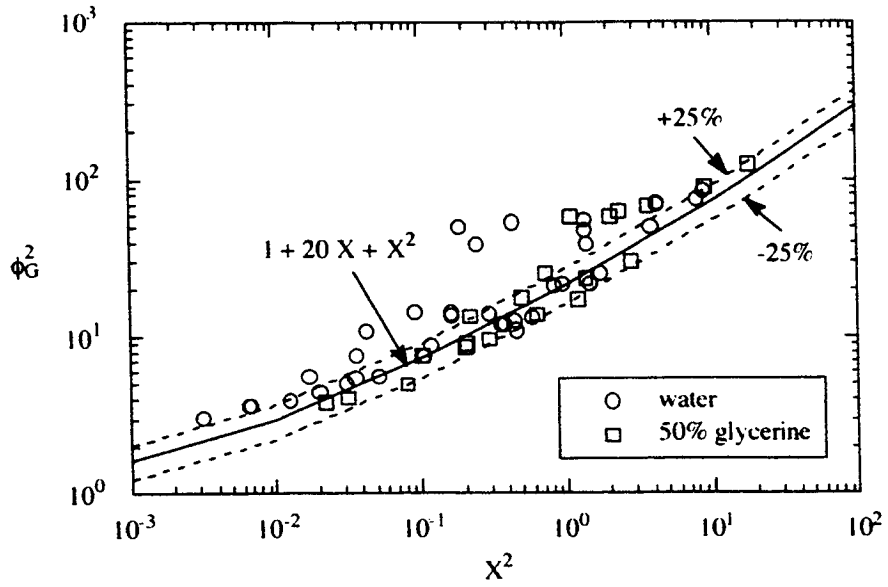

Figure 20. Comparison of measured pressure gradient with Lockhart-Martinelli correlation for annular flow

The laminar model for δ, eq.(3), applies in general for Re less than about 1600. For larger Re (>1600 or so on the ground), δ increases more rapidly with Re, due to increased waviness and turbulence. Several correlations have been proposed for δ in annular flow at earth-normal gravity. δ is correlated in terms of the friction velocity, $u* = \sqrt{(\tau/\rho)}$ as

$$\delta^+ = \frac{\delta u^*}{\nu} = f(Re) \tag{11}$$

Strictly, the correlation (11) requires knowledge of the film flow rate, the feed minus entrained droplet flow. However, for the purpose here, all of the liquid is assumed to travel in the film and the Re is assigned an additional uncertainty of 10%. The measured mean δ, normalized in this way, is plotted in Figure 21. Although there is significant scatter, the points do follow a general trend consistent with Bousman's (1994) findings in a 12.7 mm ID tube. The laminar equation,

$$d^+ = \sqrt{(Re/2)}, \tag{12}$$

and Kosky's (1971) relation,

$$d^+ = 0.0504\ Re^{7/8}, \tag{13}$$

are included for comparison, along with Bousman's fit,

$$\delta^+ = 2.65\,Re^{0.695}. \tag{14}$$

Some of the scatter in Figure 21 is due to conditions near U_{GS}=5 m/s, where the pressure drop is larger than that expected for typical annular flows. A significant number of points for Re greater than 1600 agree reasonably well with the Kosky relation, while the agreement with the laminar relation for Re<1600 is not quite as good. Bousman's low-Re data agree more closely, which may be due to random or bias errors in the current set of data.

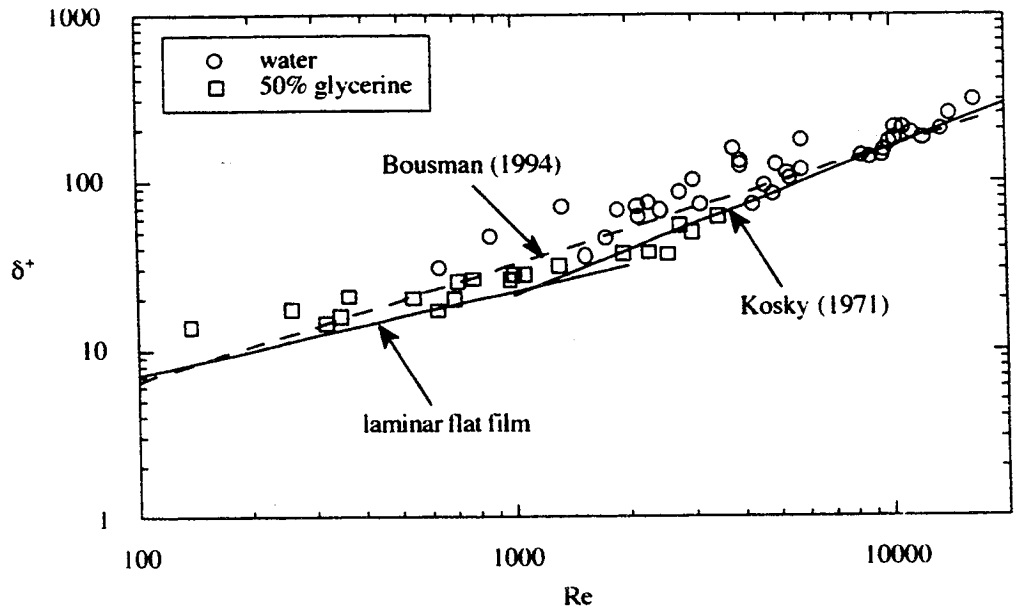

Figure 21. Correlation of experimental film thickness with liquid Reynolds number for annular flow

Slug Flow

Data Reduction: The output of the conductance probe circuit is related directly to the amount of conducting liquid between the void fraction wires, the equivalent height of which is represented by δ. The instantaneous line-average fraction of the diameter filled with liquid is then simply δ/D. For homogeneous conditions, where the bubbles or voids are distributed uniformly across the diameter, the local void fraction is simply

$$\alpha = \left(1 - \frac{\delta}{D}\right). \tag{15}$$

For separated flows, as in annular flow or along a Taylor bubble in slug flow, where the liquid occupies a contiguous region adjacent to the wall, the local void fraction, α, is equal to

$$\alpha = \left(1 - \frac{\delta}{D}\right)^2. \tag{16}$$

Full liquid pipe flow is used as a reference to account for temperature-dependent conductivity changes among runs. For slug flows, eq. (15) applies for the liquid slugs when bubbles are present, and eq. (16) applies for the Taylor bubbles. For the present conditions, the Taylor bubbles represent most of the α, so eq. (16) is more accurate and thus was used to calculate α.

Pressure Gradient Correlation: Neither of the two most commonly used techniques for correlating pressure gradient in slug flows, the Lockhart-Martinelli, 1949, method, or the homogeneous method, Wallis, 1969, correlated the present slug flow data well. A correlation of the form suggested by Chu and Jones, 1980, using the two-phase Re, Re_{TP}, was used to correlate the data

$$Re_{TP} = \frac{Re_L}{(1-\alpha)} \tag{17}$$

The equivalent liquid velocity is $U_L = U_{LS}/(1-\alpha)$ and the two-phase friction factor is

$$f_{TP} = -\frac{D}{2}\frac{\nabla P}{\rho_L U_L^2} \tag{18}$$

This formulation correlates very well with the Re_{TP} for both water and 50% glycerine. However the ratio of gas-to-liquid kinematic viscosity, $(\nu_G/\nu_L)^2$, is required for both fluids to follow the same dependence on Re_{TP}, as given below in eq. (19).

$$f_{TP} = \frac{14,500}{Re_{TP}^{1.92}}\left(\frac{\nu_G}{\nu_L}\right)^2 \tag{19}$$

but experiments over extended conditions and with other fluids are needed to justify the empirical inclusion of the viscosity ratio.

Correlation of Heat Transfer: In a manner similar to that used for annular flows, the steady wall temperatures were estimated. T_w's were placed in the dimensionless form,

$$\theta_w = \frac{T_w - T_{IN}}{q_w D/k}, \tag{20}$$

where T_{IN} is the inlet temperature, q_w is the mean wall heat flux, and k is the thermal conductivity. The distance along the tube, x, was normalized using Re ($Re=4G/\mu$) and Pr ($Pr=C_p\mu/k$) as

$$\xi = \frac{4x/D}{Re\,Pr}. \tag{21}$$

Assuming a uniform heat flux, the Nu ($Nu=hD/k$) based on the tube diameter is simply

$$Nu = \frac{1}{\theta_w - \theta_B}, \tag{22}$$

from which the heat transfer coefficient, h, was back-calculated for each run. T_B was estimated from an enthalpy balance on the liquid as

$$T_B = T_{IN} + \frac{q_w x}{\Gamma C_p}, \tag{23}$$

from which the simplification, $q_B = \xi$, results.

Several local Nu calculated with eq. (22) are shown in Fig. 22. The leading digits, 6 and 7, in the run number indicate water and 50% glycerine, respectively. The larger Nu correspond to wall-to-bulk ΔT's that are smaller and more difficult to measure accurately. However, the scatter is relatively small along the heated length and the asymptotic Nu fairly easy to interpret from an average taken near the tube exit. In the case of obvious deviations from the norm, as in the case when wall temperatures were far from their steady values, local measurements were discarded from the average.

Chu and Jones (1980) used the two-phase Reynolds number from equation (16) to correlate two-phase Nusselt number in a form similar to the Sieder-Tate, 1936, correlation. The form of their correlation is

$$Nu = A\,Re_{TP}^{n}\,Pr^{1/3}\left(\frac{Pr}{Pr_w}\right)^{0.14}\left(\frac{P_a}{P}\right)^{0.17}, \tag{24}$$

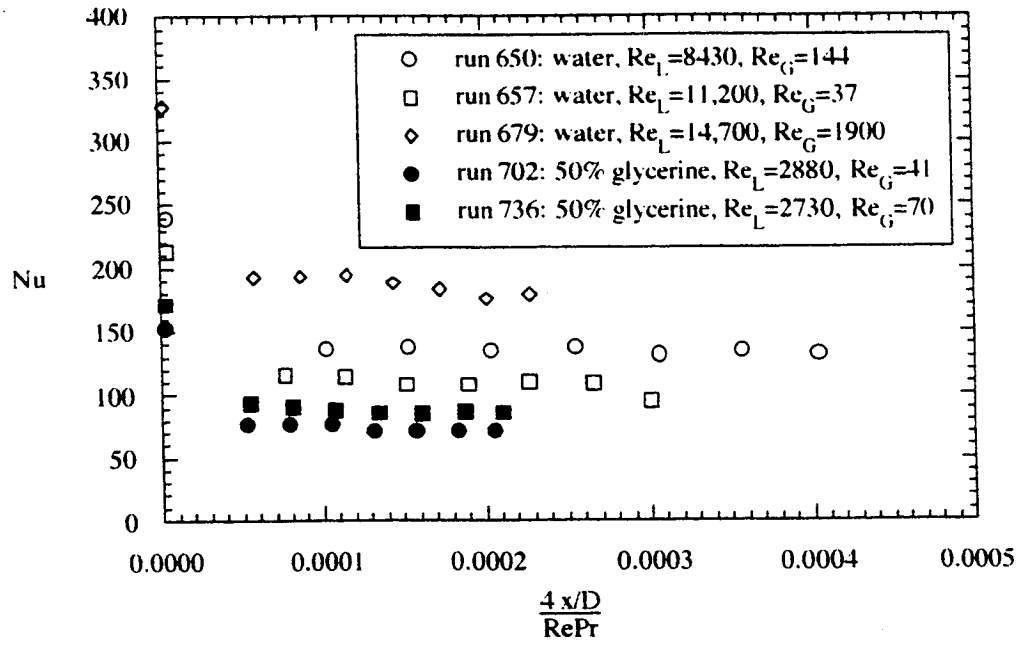

Figure 22. Typical local Nusselt number along heated length for slug flow

where Pr_w is the wall Pr, P_a is atmospheric pressure and P is the local pressure. For the Chu and Jones experiments, n=0.55 for both vertical upflows and downflows. The constant, A, varies slightly between upflow and downflow as 0.43 and 0.47, respectively. The current data were compared with the Chu and Jones correlations. The best fit occurs for A=0.14 and n=0.62. The comparison also implied lower heat transfer coefficients under reduced gravity, although the Chu and Jones data were collected over the higher range of Re_{TP} between 40,000 and 600,000. The current data approach the Chu and Jones correlation at larger two-phase Reynolds numbers of around 60,000, but the differences are significant.

A new correlation for the present experiments was obtained with the unmodified Re and the Nu modified with the term, $\sqrt{(1-\alpha)}$. This term can be viewed as a multiplier to obtain an equivalent tube diameter based on the liquid velocity, U_L. By equating liquid volume fluxes using U_L and U_{LS} as

$$U_{LS}D^2 = U_L D_e^2, \tag{25}$$

one finds that $D_e=D\sqrt{(1-\alpha)}$, and the equivalent Nu based on this diameter is $Nu\sqrt{(1-\alpha)}$. This Nu is correlated in the form of

$$Nu\sqrt{1-\alpha} = A\,Re_L^n\,Pr^{1/3}\left(\frac{Pr}{Pr_w}\right)^{1/4}, \qquad (26)$$

in Figure 23. Nearly all of the data fall within ±20% of eq.(26) with A=0.154 and n=0.61. Data at higher liquid Re are needed to extend and improve the confidence in the correlations obtained with eqs. (24) and (26), both of which appear to be adequate for the limited range of conditions studied here.

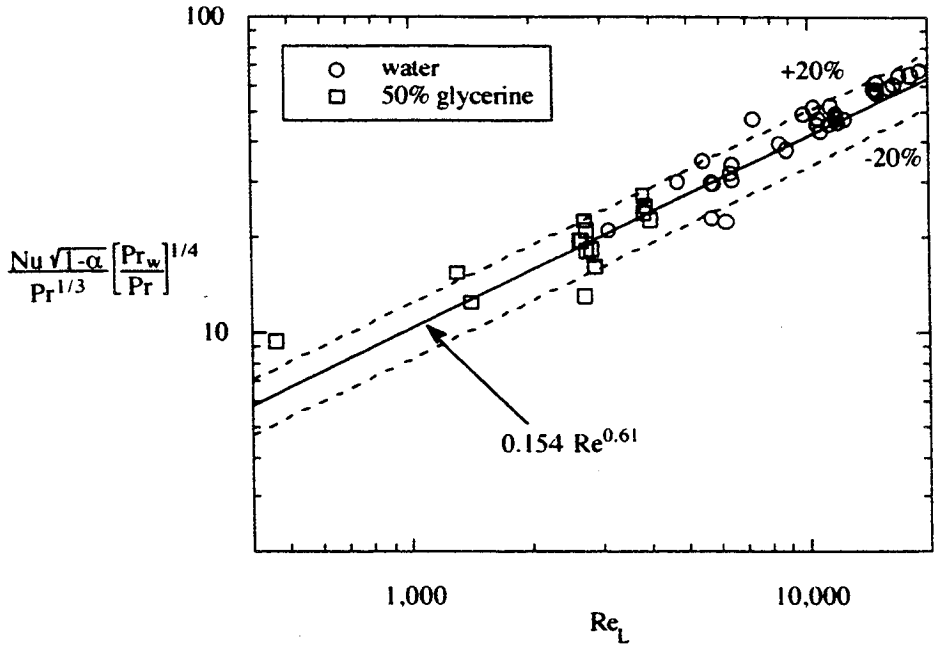

Figure 23. Correlation of overall heat transfer for slug flow

SUMMARY OF HEAT TRANSFER RESEARCH

For annular gas-liquid flows of air-water and air-50% glycerine under reduced gravity conditions, the pressure gradient agrees fairly well with a version of the Lockhart-Martinelli correlation but the measured film thickness deviates from published correlations at lower Reynolds numbers. Nusselt numbers, based on a film thickness obtained from standard normal-gravity correlations, follow the relation, $Nu = A\,Re^n\,Pr^{1/3}$, but more experimental data in a reduced gravity environment are needed to increase the confidence in the estimated constants, A and n.

In the slug flow regime, experimental pressure gradient does not correlate well with either the Lockhart-Martinelli or a homogeneous formulation, but does correlate nicely

with a formulation based on a two-phase Reynolds number. Comparison with ground-based correlations implies that the heat transfer coefficients are lower at reduced gravity than at normal gravity under the same flow conditions. Nusselt numbers can be correlated in a fashion similar to Chu and Jones.

ACKNOWLEDGMENT

This research was supported by the NASA Lewis Research Center under grant NAG3-510. Special thanks are due to the Lewis team of J. McQuillan, G. Fedor, S. Fisher, T. Lorik and M. Shoemaker, and to R. Mate at the University of Houston. Thanks are also extended to Prof. Abe Dukler (posthumously) for being the originator of this research.

REFERENCES

Andreussi, P. and Zanelli, S. 1979 "Downward Annular and Annular-Mist Flow of Air-Water Mixtures," in Two-Phase Mass, Momentum, and Heat Transfer in Chemical Process and Engineering Systems, F. Durst, G. V. Tsiklauri and N. Afgan, Eds., Hemisphere, Washington.

Bousman, W. S. 1995 "Studies of Two-Phase Gas-Liquid Flow in Microgravity", NASA Contractor Report 195434, also PhD Dissertation, University of Houston, 1994.

Bousman, W. S. and Dukler, A. E. 1994 "Ground Based Studies of Gas-Liquid Flows in Microgravity Using Lear Jet Trajectories," Paper AIAA 94-0829, 32nd Aerospace Sciences Meeting and Exhibit, Reno, NV.

Chisholm, D. and Laird, A. D. M. 1958 "Two-Phase Flow in Rough Tubes," *Trans. ASME*, **80** (2), 276-286.

Colin, C., 1990 "Ecoulements Diphasiques a Bulles et a Poches en Micropesanteur", MS Thesis, Institut de Mechaniques des Fluides de Toulouse, France.

Dukler, A. E., Fabre, J. A., McQuillen, J. B. and Vernon, R. 1988 "Gas-Liquid Flow at Microgravity Conditions: Flow Patterns and Their Transitions," *Int. J. Multiphase Flow*, **14**, 389-400.

Chu, Y-C., and Jones, B. G. 1980 "Convective Heat Transfer Coefficient Studies in Upward and Downward, Vertical, Two-Phase, Non-Boiling Flows," *AIChE Symp. Series*, **76**, 79-90.

Huckerby, C. S., and Rezkallah, K.S. 1992 "Flow Pattern Observations in Two-Phase Gas-Liquid Flow in a Straight Tube under Normal and Microgravity Conditions", Proc.of the 1992 AIChE Heat Transfer Conference, **88,** 288, San Diego, pp. 139-147.

Janicot, A. J. P. 1988 "Experimental and Theoretical Studies of Gas-Liquid Two-Phase Flow at Reduced Gravity Conditions, MS Thesis, University of Houston.

Kosky, P. G. 1971 "Thin Liquid Films Under Simultaneous Shear and Gravity Forces", *Int. J. Heat Mass Transfer*, **14**, 1220-1224.

Lacy, C. E. 1992, "Flooding and Wavy Films in Vertical Annular Gas-Liquid Flows", PhD Dissertation, University of Houston.

Lockhart, L. W. and Martinelli, R. C. 1949 "Proposed Correlation of Data of Isothermal Two-Phase, Two Component Flow in Pipes," *Chem. Engng. Prog.*, **45**, 39-48.

McQuillen, J. B. and Neumann, E. S. 1995, "Two-Phase Flow Research Using the Learjet Apparatus", NASA Technical Memorandum 106814, NASA-Lewis Research Center.

Rezkallah, K. S. and Sims, G.E. 1987 "An Examination of Correlations of Mean Heat-Transfer Coefficients in Two-Phase Two-Component Flow in Vertical Tubes," *AIChE Symp. Ser.*, **83** (257), 109-114.

Shah, M. M., 1981 "Generalized Prediction of Heat Transfer During Two Component Gas-Liquid Flow in Tubes and Other Channels," *AIChE Symp. Ser. 208*, **77**, 141-151.

Sieder, E. N. and Tate, G. E. 1936 "Heat Transfer and Pressure Drop of Liquids in Tubes," *Ind. Eng. Chem.*, **28** (12), 1428.

Wallis, G. B. 1969, One Dimensional Two-Phase Flow, McGraw-Hill, New York.

Zhao, L. and Rezkallah, K. S. 1993, "Gas-Liquid Flow Patterns at Microgravity Conditions," *Int. J. Multiphase Flow*, **19**, 751-763.

Zuber, N. and Findlay, J.A. 1965, "Average Volumetric Concentration in Two Phase Systems, *J. Ht. Trans.*, pp. 453-468.

NOMENCLATURE

A	correlation constant
C_p	specific heat
D	tube diameter
f	friction factor
f_{TP}	two-phase friction factor
h	heat transfer coefficient
k	thermal conductivity
n	correlation power
Nu	Nusselt number
Pr	Prandtl number
q_w	wall heat flux
Re	Reynolds number

We	Weber number
x	axial coordinate
X	Lockhart-Martinelli parameter
α	void fraction
δ	film thickness
ϕ_L^2	Lockhart-Martinelli multiplier
∇P	pressure gradient
Γ	mass flow per unit perimeter
σ	surface tension
ρ_l	liquid density
τ	shear stress
μ	viscosity
ν	kinematic viscosity
ρ	density
ξ	dimensionless axial coordinate
θ	dimensionless temperature

subscripts

B	bulk
G	gas
L	liquid
S	superficial
TP	two-phase
W	wall

APPENDIX I. PUBLICATIONS RESULTING FROM GRANT

Bousman, W. S. 1995 "Studies of Two-Phase Gas-Liquid Flow in Microgravity", NASA Contractor Report 195434, also PhD Dissertation, University of Houston, 1994.

Bousman, W. S. and Dukler, A. E. 1994 "Ground Based Studies of Gas-Liquid Flows in Microgravity Using Lear Jet Trajectories," Paper AIAA 94-0829, 32nd Aerospace Sciences Meeting and Exhibit, Reno, NV.

Bousman, W. S. and Dukler, A. E., 1993, "Studies of Gas-Liquid Flow in Microgravity: Void Fraction, Pressure Drop and Flow Patterns", presented at the ASME Winter Annual Meeting, New Orleans.

Bousman, W. S., Witte, L. C. and McQuillen, J. B. 1996, "Gas-Liquid Flow Patterns in Microgravity: Effects of Tube Diameter, Liquid Viscosity and Surface Tension", accepted for International Journal of Multiphase Flow.

Fore, L. B., Witte, L. C. and McQuillen, J. B., 1996, "Heat Transfer to Annular Gas-Liquid Mixtures at Reduced Gravity", submitted to Journal of Thermophysics and Heat Transfer, (Dec., 1995).

Fore, L. B., Witte, L. C. and McQuillen, J. B., 1996, "Thermal Hydraulics of Two Phase Slug Flow under Reduced Gravity", submitted to Int. Journal of Multiphase Flow, (Jan., 1996).

Fore, L. B., Bousman, W. S. and Witte, L. C. 1996, "Two-Phase Flow Dynamics and Heat Transfer in Microgravity", to be presented at the Energy Week Conference and Exhibit, Houston, TX, Jan. 1996.

Fore, L. B. and Witte, L. C. 1995, "Roll Wave Effects on the Heating of Viscous Liquid Films", presented at the National Heat Transfer Conference, Portland, OR, August, 1995. Published in ASME HTD Vol. 314, pp. 23-30.

Fore, L. B., Witte, L. C. and McQuillen, J. B. 1996, "Microgravity Heat Transfer and Pressure Drop in Gas-Liquid Mixtures: Slug and Annular Flow", to be presented at the National Heat Transfer Conference, Houston, TX.

Table II. 1

Microgravity Water Experiments

run #	U_{GS} m/s	U_{LS} m/s	pattern	press. psi	film probe δ/R	film probe rms	void probe δ/D	void probe rms	dp/dz Pa/m	void fraction	h W/m^2C	$Re(T_B)$	Pr	Pr_w
601	11.2	0.140	annular	17.6	0.097	0.032	0.105	0.052	1173					
602	11.2	0.140	annular	17.6	0.100	0.032	0.097	0.051	1232		4063	4889	5.0	4.5
604	23.2	0.080	annular	23.3	0.052	0.024	0.051	0.024	1603		3614	2732	5.1	4.5
606	15.8	0.170	annular	18.7	0.089	0.031	0.088	0.042	1498		5140	4956	6.1	5.5
609	4.9	0.195	annular	16.5	0.134	0.041	0.143	0.076	1059		3750	5808	5.9	5.2
610	15.0	0.350	annular	20.2	0.112	0.031	0.120	0.052	2088		6610	10325	6.0	5.5
613	22.4	0.130	annular	24.6	0.060	0.025	0.093	0.026	2004					
615	10.0	0.478	annular	18.5	0.124	0.036	0.154	0.062	1834		6340	14335	5.9	5.4
618	4.8	0.550	annular	17.0	0.154	0.060	0.199	0.088	1571		5630	16592	5.8	5.3
619	23.4	0.026	annular	23.3	0.027	0.014	0.028	0.012	1251		3000	634	7.4	6.4
622	10.8	0.096	annular	16.7	0.072	0.025	0.069	0.035	1128		3720	2770	6.1	5.3
624	15.9	0.088	annular	17.8	0.056	0.023	0.054	0.029	1241		2800	2463	6.3	5.6
625	5.0	0.103	annular	15.5	0.098	0.034	0.088	0.045	977		2750	3001	6.1	5.0
627	14.7	0.295	annular	18.6	0.090	0.025	0.094	0.043	1766		6047	9662	5.3	4.9
630	21.8	0.165	annular	23.3	0.060	0.023	0.058	0.028	2022		6060	4638	6.3	5.8
632	4.9	0.366	annular	16.4	0.134	0.052	0.151	0.079	1287		4800	10845	6.0	5.3
634	10.3	0.348	annular	17.8	0.104	0.032	0.118	0.054	1614		6020	10252	6.0	5.5
636	14.5	0.389	annular	19.7	0.103	0.028	0.115	0.045	2028		6850	11399	6.0	5.6
637	23.1	0.040	annular	27.0										
645	18.6	0.036	annular	22.7	0.031	0.014	0.049	0.016	977		5200	866	7.5	6.8
648	18.0	0.080	annular	22.8	0.048	0.020	0.054	0.025	1115					
651	10.8	0.216	annular	17.7	0.127	0.053	0.110	0.044	973		5197	6723	5.7	5.1

Table II.1, cont.

656	10.2	0.300	annular	17.9							5835	9159	5.8	5.3
658	4.9	0.350	annular	16.9	0.180	0.093	0.133	0.073	950		4960	9571	6.5	5.8
660	4.9	0.200	annular	16.5	0.148	0.074	0.110	0.062	742		3920	5429	6.6	5.7
661	19.5	0.116	annular	21.5	0.061	0.028	0.055	0.022	1502					
663	5.2	0.080	annular	16.4	0.094	0.041	0.073	0.040	807		2670	2136	6.7	5.4
666	21.0	0.050	annular	27.3	0.044	0.023	0.056	0.017	1407					
667	10.4	0.181	annular	17.5	0.093	0.042	0.075	0.039	1067					
669	21.2	0.050	annular	27.0										
672	16.0	0.162	annular	18.8	0.076	0.033	0.059	0.029	1327		5800	4279	6.8	6.1
675	5.0	0.197	annular	16.4	0.134	0.070	0.106	0.054	912		4080	5326	6.6	5.8
676	15.2	0.360	annular	20.4	0.104	0.039	0.102	0.036	1864		7080	9674	6.6	6.1
680	10.1	0.450	annular	19.3	0.132	0.058	0.129	0.050	1669		6680	12211	6.6	6.0
683	4.6	0.500	annular	17.5	0.196	0.122	0.160	0.080	1316		5170	13610	6.5	5.8
688	10.8	0.068	annular	17.2	0.066	0.032	0.048	0.025	870		3420	1753	6.9	5.9
690	16.5	0.063	annular	18.6	0.047	0.025	0.036	0.020	1017		3920	1548	7.3	6.3
691	5.1	0.073	annular	16.3	0.091	0.045	0.065	0.036	981		2600	1889	6.9	5.6
696	4.9	0.368	annular	16.7	0.178	0.118	0.135	0.073	1339		4990	9914	6.6	5.9
698	10.4	0.330	annular	18.3	0.116	0.050	0.100	0.046	1630		6030	8837	6.7	6.0
603	2.0	0.155	slug	16.0	0.169	0.076	0.161	0.094	929	0.71	2527	4666	5.9	4.8
605	0.2	0.212	slug	15.5	0.634	0.245	0.485	0.386	1028	0.41	1908	6373	5.9	4.6
607	0.4	0.214	slug	15.6	0.419	0.306	0.335	0.343	1037	0.56	2078	6425	5.9	4.7
608	1.0	0.214	slug	15.9	0.203	0.158	0.209	0.183	1053	0.66	2634	6425	5.9	4.9
611	0.2	0.528	slug	15.5	0.680	0.301	0.598	0.330	1164	0.27	3117	15843	5.9	5.0
612	0.3	0.544	slug	15.4	0.668	0.304	0.600	0.333	1040	0.27	3169	16367	5.9	5.0
614	1.0	0.557	slug	15.8	0.279	0.247	0.311	0.269	1170	0.55	4250	16772	5.9	5.2
616	0.4	0.595	slug	15.0	0.490	0.322	0.495	0.351	1068	0.38	3667	17960	5.8	5.1

Table II.1, cont.

617	1.9	0.574	slug	16.0	0.208	0.146	0.243	0.168	1447	0.60	4594	18979	5.3	4.8
620	1.1	0.211	slug	15.0	0.189	0.156	0.180	0.166	1119	0.70	1889	6209	6.0	4.6
621	0.2	0.076	slug	14.8										
623	0.4	0.107	slug	14.8	0.364	0.275	0.255	0.277	1024	0.63				
626	2.0	0.106	slug	15.0	0.123	0.057	0.126	0.082	904	0.77	2011	3113	6.0	4.7
628	1.0	0.390	slug	15.0	0.234	0.247	0.256	0.241	1125	0.61	3400	11648	5.9	5.1
629	0.4	0.392	slug	14.9	0.501	0.379	0.442	0.397	1074	0.47	3016	11638	6.0	5.0
631	2.0	0.380	slug	15.7	0.181	0.135	0.199	0.147	1198	0.66	3979	11285	5.9	5.2
633	0.2	0.398	slug	14.9	0.668	0.322	0.559	0.373	1050	0.33	2562	11826	5.9	4.9
635	2.0	0.498	slug	15.9	0.197	0.148	0.224	0.160	1375	0.63	4452	14781	6.0	5.3
638	0.8	0.166	slug	15.6	0.168	0.200	0.182	0.187	694	0.70				
639	2.0	0.164	slug	16.0	0.132	0.094	0.128	0.086	243	0.77				
643	0.8	0.070	slug	15.4										
644	0.2	0.067	slug	15.4										
647	2.0	0.065	slug	15.8										
649	0.2	0.323	slug	15.3										
650	0.8	0.305	slug	15.6	0.237	0.264	0.228	0.257	914	0.66	3117	8433	6.4	5.4
652	1.9	0.265	slug	16.0	0.234	0.188	0.176	0.131	652	0.70	3896	7240	6.5	5.6
654	0.4	0.280	slug	15.5	0.711	0.533	0.366	0.386	969	0.55				
655	0.3	0.410	slug	15.5										
657	0.2	0.410	slug	15.3	1.107	0.422	0.565	0.385	905	0.34	2597	11236	6.5	5.3
659	1.0	0.280	slug	15.6	0.336	0.372	0.215	0.236	973	0.67	2925	8709	5.7	4.8
662	1.0	0.071	slug	15.8										
664	0.4	0.092	slug	15.4										
665	2.0	0.356	slug	16.2	0.240	0.186	0.174	0.118	974	0.70	4065	9693	6.5	5.7
668	2.0	0.200	slug	16.0	0.191	0.148	0.143	0.094	769	0.74	3169	5447	6.5	5.5

TAble II.1, cont.

670	0.2	0.210	slug	15.6										
671	0.2	0.210	slug	15.4	0.715	0.476	0.422	0.332	950	0.44	1484	5704	6.6	4.6
673	0.4	0.210	slug	15.4	0.647	0.490	0.331	0.337	973	0.56	2101	5743	6.5	5.0
674	1.0	0.210	slug	15.6	0.267	0.281	0.181	0.168	999	0.70	2527	5720	6.5	5.3
677	0.2	0.540	slug	15.6	0.995	0.489	0.606	0.336	973	0.27	3066	14780	6.5	5.4
679	1.0	0.540	slug	16.2	0.379	0.394	0.292	0.249	1106	0.56	4250	14721	6.5	5.7
681	0.4	0.540	slug	16.0	0.704	0.570	0.481	0.368	1014	0.40	3463	14762	6.5	5.5
682	2.0	0.530	slug	16.6	0.273	0.238	0.214	0.158	1247	0.64	4452	14475	6.5	5.7
685	1.0	0.400	slug	15.7	0.321	0.348	0.245	0.222	1062	0.62	3371	12255	5.8	5.0
686	1.0	0.092	slug	15.5	0.221	0.222	0.137	0.122	965	0.76				
687	0.2	0.077	slug	15.2										
689	0.4	0.077	slug	15.3	0.472	0.450	0.233	0.300	1000	0.68				
692	2.1	0.075	slug	15.5	0.119	0.084	0.106	0.068	734	0.80				
693	1.0	0.388	slug	15.5	0.346	0.373	0.234	0.241	1067	0.65	3528	10473	6.6	5.6
694	0.4	0.390	slug	15.3	0.610	0.565	0.403	0.369	1126	0.49	3066	10546	6.6	5.5
695	2.0	0.378	slug	16.2	0.242	0.207	0.196	0.141	1212	0.67	4065	10215	6.6	5.7
697	0.2	0.396	slug	15.2	0.982	0.507	0.564	0.386	1057	0.34	2493	10712	6.6	5.3

Table II.2

Microgravity 50% Glycerine Experiments

run #	U_{GS} m/s	U_{LS} m/s	pattern	press. psi	film probe δ/R	film probe rms	void probe δ/D	void probe rms	dp/dz Pa/m	void fraction	h W/m^2C	$Re(T_B)$	Pr	Pr_w
701	10.8	0.384	annular	18.6	0.146	0.049	0.120	0.046	2016		3180	2382	37.1	29.6
703	4.7	0.420	annular	17.2	0.213	0.124	0.175	0.076	1626		2310	3277	29.3	22.7
705	20.0	0.080	annular	30.0										
709	14.7	0.330	annular	20.2	0.128	0.036	0.113	0.037	2211		3390	2050	37.1	29.9
710	15.9	0.058	annular	18.7	0.092	0.021	0.061	0.019	1303		2400	427	31.1	24.1
711	11.3	0.063	annular	17.5	0.099	0.025	0.071	0.025	1197		2010	452	32.0	23.5
712	22.5	0.030	annular	25.0	0.069	0.010	0.064	0.007	1576		2790	211	32.6	25.9
713	4.9	0.066	annular	16.2	0.126	0.042	0.097	0.042	1073		1600	465	32.5	22.3
714	4.4	0.585	annular	18.0	0.215	0.123	0.192	0.094	2082		2760	3580	37.7	29.0
717	10.0	0.500	annular	20.0	0.155	0.055	0.145	0.051	2367		3240	3055	37.7	30.1
719	20.0	0.100	annular	29.5	0.087	0.020	0.074	0.018	1884		3170	648	35.5	28.5
721	13.8	0.440	annular	21.0	0.134	0.041	0.107	0.040	2510		3520	2647	38.3	31.0
722	21.8	0.045	annular	29.0	0.070	0.012	0.061	0.009	1769					
723	4.9	0.138	annular	16.3	0.146	0.059	0.117	0.050	1142		1800	894	35.5	24.7
724	10.5	0.125	annular	17.3	0.112	0.033	0.083	0.034	1351		2300	798	36.0	26.8
725	15.8	0.115	annular	18.7	0.098	0.024	0.068	0.024	1555		2670	731	36.2	27.9
726	5.0	0.229	annular	16.3	0.159	0.073	0.130	0.061	1302		2080	1438	36.7	26.4
729	16.3	0.175	annular	18.9	0.110	0.031	0.094	0.028	1770		3000	1080	37.3	29.4
732	10.8	0.191	annular	17.1	0.123	0.040	0.094	0.038	2025		2680	1161	37.9	29.0
733	17.8	0.180	annular	25.6	0.105	0.029	0.088	0.024	2333		1937	1088	38.1	26.6
739	5.0	0.127	annular	16.3	0.147	0.060	0.114	0.049	1129		1810	816	35.8	24.9
702	0.2	0.456	slug	15.6	0.854	0.554	0.596	0.354	1097	0.29	1191	2875	36.6	21.6

Table II.2, cont.

704	1.9	0.435	slug	16.5	0.292	0.245	0.231	0.165	1427	0.62	2177	2706	37.1	27.0
706	0.4	0.452	slug	15.5	0.639	0.547	0.467	0.357	1117	0.41	1293	2862	36.4	22.2
707	0.4	0.445	slug	15.5	0.624	0.537	0.466	0.349	1115	0.41	1456	2804	36.5	23.4
708	1.0	0.435	slug	16.1	0.439	0.373	0.308	0.239	1150	0.54	1851	2733	36.7	25.5
715	2.0	0.620	slug	16.8	0.332	0.273	0.272	0.184	1669	0.56	2432	3805	37.6	28.1
716	0.4	0.650	slug	16.0	0.742	0.533	0.560	0.347	1163	0.31	1672	3995	37.5	25.0
718	0.9	0.630	slug	16.2	0.504	0.397	0.373	0.260	1246	0.46	2055	3882	37.4	26.7
720	0.2	0.660	slug	15.4	0.934	0.524	0.674	0.342	1119	0.22				
728	0.4	0.220	slug	15.3	0.485	0.537	0.373	0.348	1078	0.51	1120	1401	36.2	20.9
730	0.2	0.218	slug	15.0										
731	2.0	0.214	slug	15.6	0.212	0.160	0.182	0.122	1734	0.68	1685	1301	38.0	25.3
734	0.8	0.442	slug	15.2	0.438	0.403	0.334	0.268	1373	0.52	1716	2660	38.4	25.7
735	0.1	0.448	slug	15.0	0.947	0.530	0.689	0.347	1095	0.22	957	2708	38.1	20.0
736	0.4	0.446	slug	15.2	0.618	0.521	0.455	0.347	1123	0.42	1472	2730	37.7	24.0
737	1.0	0.434	slug	15.5	0.393	0.390	0.308	0.259	1169	0.55	1781	2620	38.2	26.0
738	1.9	0.063	slug	15.8	0.158	0.089	0.145	0.069	951	0.74	1094	456	31.7	19.0
740	0.8	0.646	slug	15.8	0.495	0.394	0.373	0.260	1260	0.46	1989	3825	39.0	27.3

REPORT DOCUMENTATION PAGE

Form Approved
OMB No. 0704-0188

Public reporting burden for this collection of information is estimated to average 1 hour per response, including the time for reviewing instructions, searching existing data sources, gathering and maintaining the data needed, and completing and reviewing the collection of information. Send comments regarding this burden estimate or any other aspect of this collection of information, including suggestions for reducing this burden, to Washington Headquarters Services, Directorate for Information Operations and Reports, 1215 Jefferson Davis Highway, Suite 1204, Arlington, VA 22202-4302, and to the Office of Management and Budget, Paperwork Reduction Project (0704-0188), Washington, DC 20503.

1. AGENCY USE ONLY (*Leave blank*)	2. REPORT DATE	3. REPORT TYPE AND DATES COVERED
	February 1996	Final Contractor Report

4. TITLE AND SUBTITLE

Studies of Two-Phase Flow Dynamics and Heat Transfer at Reduced Gravity Conditions

5. FUNDING NUMBERS

WU–694–03–0A
G–NAG3–510

6. AUTHOR(S)

Larry C. Witte, W. Scott Bousman, and Larry B. Fore

7. PERFORMING ORGANIZATION NAME(S) AND ADDRESS(ES)

University of Houston
Department of Chemical Engineering
Houston, Texas 77204–4792

8. PERFORMING ORGANIZATION REPORT NUMBER

E–10136

9. SPONSORING/MONITORING AGENCY NAME(S) AND ADDRESS(ES)

National Aeronautics and Space Administration
Lewis Research Center
Cleveland, Ohio 44135–3191

10. SPONSORING/MONITORING AGENCY REPORT NUMBER

NASA CR–198459

11. SUPPLEMENTARY NOTES

Project Manager, John B. McQuillen, Space Experiments Division, NASA Lewis Research Center, organization code 6712, (216) 433–2876.

12a. DISTRIBUTION/AVAILABILITY STATEMENT

Unclassified - Unlimited
Subject Category 34

This publication is available from the NASA Center for Aerospace Information, (301) 621–0390.

12b. DISTRIBUTION CODE

13. ABSTRACT (*Maximum 200 words*)

The ability to predict gas-liquid flow patterns is crucial to the design and operation of two-phase flow systems in the microgravity environment. Flow pattern maps have been developed in this study which show the occurrence of flow patterns as a function of gas and liquid superficial velocities as well as tube diameter, liquid viscosity and surface tension. The results have demonstrated that the location of the bubble-slug transition is affected by the tube diameter for air-water systems and by surface tension, suggesting that turbulence-induced bubble fluctuations and coalescence mechanisms play a role in this transition. The location of the slug-annular transition on the flow pattern maps is largely unaffected by tube diameter, liquid viscosity or surface tension in the ranges tested. Void fraction-based transition criteria were developed which separate the flow patterns on the flow pattern maps with reasonable accuracy. Weber number transition criteria also show promise but further work is needed to improve these models. For annular gas-liquid flows of air-water and air-50% glycerine under reduced gravity conditions, the pressure gradient agrees fairly well with a version of the Lockhart-Martinelli correlation but the measured film thickness deviates from published correlations at lower Reynolds numbers. Nusselt numbers, based on a film thickness obtained from standard normal-gravity correlations, follow the relation, $Nu = A\,Re^{n}\,Pr^{1/3}$, but more experimental data in a reduced gravity environment are needed to increase the confidence in the estimated constants, A and n. In the slug flow regime, experimental pressure gradient does not correlate well with either the Lockhart-Martinelli or a homogeneous formulation, but does correlate nicely with a formulation based on a two-phase Reynolds number. Comparison with ground-based correlations implies that the heat transfer coefficients are lower at reduced gravity than at normal gravity under the same flow conditions. Nusselt numbers can be correlated in a fashion similar to Chu and Jones.

14. SUBJECT TERMS

Multiphase flow; Two phase flow; Reduced gravity; Annular flow; Flow stability; Voids; Bubbles

15. NUMBER OF PAGES

40

16. PRICE CODE

A03

17. SECURITY CLASSIFICATION OF REPORT	18. SECURITY CLASSIFICATION OF THIS PAGE	19. SECURITY CLASSIFICATION OF ABSTRACT	20. LIMITATION OF ABSTRACT
Unclassified	Unclassified	Unclassified	

National Aeronautics and
Space Administration

Lewis Research Center
21000 Brookpark Rd.
Cleveland, OH 44135-3191

Official Business
Penalty for Private Use $300

POSTMASTER: If Undeliverable — Do Not Return